Received: 6 August 2021 | Revised: 30 November 2021 | Accepted: 30 November 2021

DOI: 10.1111/mmi.14855

RESEARCH ARTICLE

WILEY

Evolutionary flexibility in routes to mat formation by *Pseudomonas*

Anuradha Mukherjee | **Gunda Dechow-Seligmann** | **Jenna Gallie**

Department of Evolutionary Theory, Max Planck Institute for Evolutionary Biology, Plön, Germany

Correspondence
Jenna Gallie, Department of Evolutionary Theory, Max Planck Institute for Evolutionary Biology, 24306 Plön, Germany.
Email: gallie@evolbio.mpg.de

Present address
Anuradha Mukherjee, Institute of Experimental Medicine, Christian-Albrechts University (UKSH Campus), Kiel, Germany

Funding information
International Max Planck Research School for Evolutionary Biology; Max-Planck-Gesellschaft

Abstract

Many bacteria form mats at the air-liquid interface of static microcosms. These structures typically involve the secretion of exopolysaccharides, the production of which is often controlled by the secondary messenger c-di-GMP. Mechanisms of mat formation have been particularly well characterized in *Pseudomonas fluorescens* SBW25; stimuli or mutations that increase c-di-GMP production by diguanylate cyclases (WspR, AwsR, and MwsR) result in the secretion of cellulose and mat formation. Here, we characterize and compare mat formation in two close relatives of SBW25: *Pseudomonas simiae* PICF7 and *P. fluorescens* A506. We find that PICF7—the strain more closely related to SBW25—can form mats through mutations affecting the activity of the same three diguanylate cyclases as SBW25. However, instead of cellulose, these mutations activate production of the exopolysaccharide Pel. We also provide evidence for at least two further—as yet uncharacterized—routes to mat formation by PICF7. *P. fluorescens* A506, while retaining the same mutational routes to mat formation as SBW25 and PICF7, preferentially forms mats by a semi-heritable mechanism that culminates in Psl and Pga over-production. Our results demonstrate a high level of evolutionary flexibility in the molecular and structural routes to mat formation, even among close relatives.

KEYWORDS
biofilms, cellulose, exopolysaccharides, Pel, Psl

1 | INTRODUCTION

Many bacteria can form structures on solid surfaces (biofilms) or at the air-liquid interface of static microcosms (mats or pellicles). The formation of these structures is dependent on the production and secretion of exopolysaccharides (EPSs) by the bacterial cells. EPS production can afford bacterial cells protection against stresses such as desiccation or starvation (Davey & O'Toole, 2000), enhancing persistence in a range of environments (Costerton, 1999; Gal et al., 2003; Yaron & Römling, 2014). Given the prevalence of biofilms and mats, the evolutionary and molecular mechanisms behind their production are of interest. Here we characterize mat production in two biocontrol agents, *Pseudomonas simiae* PICF7 and *Pseudomonas fluorescens* A506, and contrast them with previously well-studied routes to mat formation in *P. fluorescens* SBW25.

The process of mat and biofilm formation often involves the concerted production of multiple structural components, and hence is under complex control. The biosynthesis of many structural components is regulated by the secondary messenger bis(3′-5′)-cyclic dimeric guanosine monophosphate (c-di-GMP) (Liang, 2015;

Römling et al., 2013; Ross et al., 1987). C-di-GMP is produced from GTP by enzymes called diguanylate cyclases (DGCs) with active GGDEF domains (Tal et al., 1998). Conversely, c-di-GMP is broken down by c-di-GMP-specific phosphodiesterases (PDEs), the activity of which is dependent on conserved EAL or HD-GYP domains (Schmidt et al., 2005). Most bacteria encode multiple DGCs and PDEs, the combined expression levels and activities of which determine local and global intracellular c-di-GMP levels.

The output of c-di-GMP from DGCs and PDEs is controlled through various signaling pathways (reviewed in Römling et al., 2013; Valentini & Filloux, 2019). Commonly, signals are transduced by two-component systems (TCSs), in which a signal activates the first component (a histidine kinase) and is passed by a phosphotransfer event to the second component (a response regulator; Nixon et al., 1986; reviewed in Stock et al., 2000). Response regulators include several c-di-GMP metabolizing enzymes, such as WspR of *P. fluorescens* (Malone et al., 2007) and PleD of *Caulobacter crescentus* (Chan et al., 2004). Notably, DGC/PDE output can be modulated in a graded, reversible manner by environmental or physiological stimuli (e.g., Ardré et al., 2019; Barends et al., 2009), or in a constitutive manner by mutations in the DGC/PDE or associated signaling pathways (e.g., Bantinaki et al., 2007; McDonald et al., 2009; Paul et al., 2004).

The downstream targets of c-di-GMP are varied; known examples fall into four categories: (i) PilZ domains (Amikam & Galperin, 2006; Lee et al., 2007; Ryjenkov et al., 2006), (ii) degenerate, enzymatically inactive GGDEF/EAL domains (Colvin et al., 2012; Duerig et al., 2009; Li et al., 2012), (iii) other, distinct c-di-GMP binding domains in transcriptional regulators (Baraquet et al., 2012; Hickman & Harwood, 2008), and (iv) mRNA riboswitches (Chen et al., 2011; Sudarsan et al., 2008). Overall, c-di-GMP regulates a large number of targets at the levels of transcription, translation, and enzymatic activity. Many EPSs are downstream targets of c-di-GMP, including cellulosic polymers in *Acetobacter xylinum*, *Escherichia coli*, and *P. fluorescens* (Goymer et al., 2006; Richter et al., 2020; Ross et al., 1987), poly-beta-1,6-N-actyl-D-glucosamine (Pga) in *E. coli* and *P. fluorescens* (Boehm et al., 2009; Lind et al., 2017; Steiner et al., 2012), and Pel in *P. aeruginosa* and *Bacillus cereus* (Hickman & Harwood, 2008; Whitfield et al., 2020).

P. fluorescens SBW25 is a model system in evolutionary biology, in which the mechanisms of mat formation have been particularly well characterized (reviewed in Koza et al., 2017; Spiers, 2014). In standard static microcosms, wild-type SBW25 cells initially produce relatively small amounts of cellulose in response to currently ill-defined stimuli, leading to fragile mats—visible with specialized equipment—at the air-liquid interface within ~20 hr of incubation (Ardré et al., 2019). Over time, mutants that constitutively produce cellulose ("wrinkly spreaders") arise and form easily visible, robust mats at the air-liquid interface within 72 hr (Bantinaki et al., 2007; Koza et al., 2011; Lind et al., 2019; McDonald et al., 2009; Rainey & Travisano, 1998). In addition, under other conditions, SBW25 is known to form mats by alternative mechanisms. In particular, SBW25 can form (i) cellulose-based mats by a non-mutational, physiological mechanism in the presence of excess iron (Koza et al., 2009, 2020) and (ii) Pga- or cell chain-based mats via mutational mechanisms when cellulose is not available (Gallie et al., 2019; Lind et al., 2017).

At the molecular level, SBW25 mat formation involves the production of c-di-GMP—as a result of physiological signaling (Ardré et al., 2019) or mutation (Bantinaki et al., 2007; Beaumont et al., 2009; Lind et al., 2017; McDonald et al., 2009)—by one of three enzymes: WspR (DGC), AwsR (DGC), or MwsR (combined DGC/PDE). Elevated c-di-GMP levels lead to the production of cellulose (Goymer et al., 2006; Spiers et al., 2003) and/or Pga (Bantinaki et al., 2007; Lind et al., 2017). In the case of cellulose, c-di-GMP is thought to target the biosynthetic machinery (Wss) by binding to the PilZ domain of WssB. The mechanism by which c-di-GMP activates SBW25 Pga has not been elucidated, but may resemble the *E. coli* mechanism of c-di-GMP binding to, and activating, Pga pathway components (Boehm et al., 2009; Steiner et al., 2012). Ultimately, c-di-GMP-mediated production of cellulose and/or Pga leads to the formation of mats at the air-liquid interface.

In this work, we characterize and compare mat formation in two relatives of *P. fluorescens* SBW25: *P. simiae* PICF7 and *P. fluorescens* A506. We find that, despite their relatively close evolutionary relationship, each strain produces mats by distinct molecular and structural mechanisms.

2 | RESULTS

2.1 | Evolutionary relationships and the genetics of EPS production

In this study, we concentrate on three *Pseudomonas* strains: (i) *P. fluorescens* SBW25, isolated from a sugar beet leaf in the United Kingdom, (ii) *P. simiae* PICF7 (formerly *P. fluorescens* PICF7), isolated from the roots of an olive plant in Spain, and (iii) *P. fluorescens* A506, isolated from a pear plant in the USA (Table S1). All three are plant growth-promoting strains, and PICF7 and A506 are biocontrol agents, respectively, for Verticillium wilt of olive (Mercado-Blanco et al., 2004) and fire blight of pear and apple (Stockwell et al., 2010). Complete genome sequences are available (Loper et al., 2012; Martínez-García et al., 2015; Silby et al., 2009), and A506 contains a sequenced, ~57 kb conjugative plasmid (pA506; Stockwell et al., 2013). Phylogenetic analyses of whole-genome alignments indicate that *P. fluorescens* SBW25 and *P. simiae* PICF7 more recently shared a common ancestor with each other than with *P. fluorescens* A506 (Figure 1).

SBW25, PICF7, and A506 encode the biosynthetic genes required to synthesize distinct sets of EPSs; each strain carries genes for Pga, Psl, and alginate biosynthesis, and SBW25 and PICF7 have the genetic capacity to synthesize additional polymers (cellulose and colanic acid in SBW25, Pel in PICF7) (Tables 1 and S2). In addition, all three strains carry homologues of the *wsp*, *aws*, and *mwsR* loci, each of which encodes a signaling pathway with at least one c-di-GMP metabolizing domain (DGC and/or PDE; Table S2). Hence, each

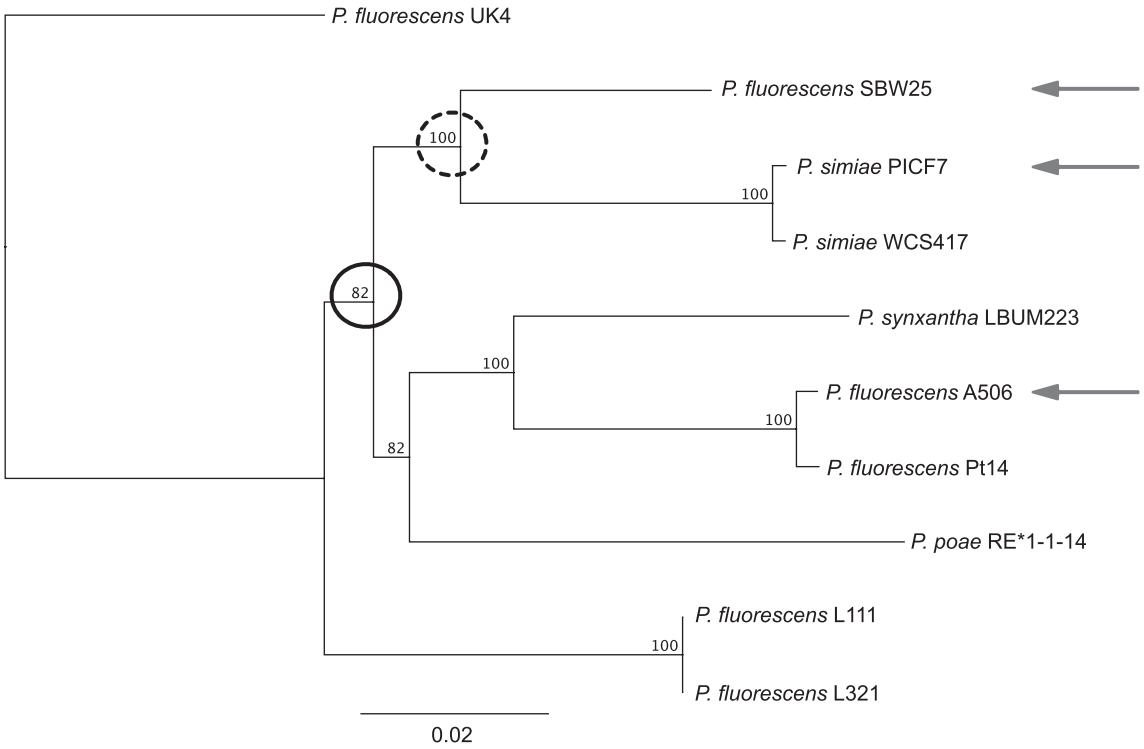

FIGURE 1 Phylogenetic tree highlighting the evolutionary relationships between *Pseudomonas fluorescens* SBW25, *Pseudomonas simiae* PICF7, and *P. fluorescens* A506. The complete genome sequences of ten pseudomonads were obtained (see Table S1). Whole genome alignments of these strains were generated using REALPHY (Bertels et al., 2014), and used to construct a maximum likelihood tree with PHYML (Guindon & Gascuel, 2003) (see also Experimental Procedures). The support shown next to the branches is based on 100 bootstrap replicates. The most divergent strain, *P. fluorescens* UK4, was used as an outgroup. The three strains of interest (*P. fluorescens* SBW25, *P. simiae* PICF7, and *P. fluorescens* A506) are indicated by grey arrows. The last common ancestor of SBW25 and PICF7 is indicated by the dotted circle, and the last common ancestor of all three by the solid circle

of SBW25, PICF7, and A506 has the genetic capacity to metabolize c-di-GMP, with a strain-specific set of possible downstream (EPS) targets.

2.2 | PICF7 and A506 form mats and diverse colony morphotypes in static microcosms

To investigate mat formation by PICF7 and A506 relative to SBW25, single (smooth, wild-type) colonies of all three strains were inoculated into separate, standard King's Medium B (KB) microcosms and incubated statically at 28°C. In accordance with previous studies (e.g., Rainey & Rainey, 2003; Rainey & Travisano, 1998), microcosms seeded by SBW25 typically formed robust mats within 48–72 hr (and did not form easily visible mats at 24 hr; Koza et al., 2009). The robust 72-hr mats remained at the air-liquid interface for ~5–10 days before detaching and sinking (Figures 2a and S1). Microcosms inoculated with PICF7 also developed robust mats within 48–72 hr, which continued to change morphologically and were often still intact after 14 days of incubation (Figures 2a and S1). In the majority of microcosms founded by A506, fragile but visible mats formed within 24 hr. By 72 hr, these became only slightly more robust, and they disappeared after 7–10 days of incubation. Overall, although each of SBW25, PICF7, and A506 is capable of forming mats at the air-liquid interface, they appear to do so in strain-specific ways.

Given that all three strains had consistently formed visible mats at 72 hr (Figure 2a), we concentrated on characterizing mat formation at this time point. Plating of cells from 72-hr static microcosms founded by each of the three strains revealed the development of diverse colony morphologies (Figure 2b). As expected, SBW25 gave rise to three distinct morphotypes (Smooth, Wrinkly Spreader, Fuzzy Spreader) (Rainey & Travisano, 1998). Five distinct morphotype classes were observed arising from the majority of PICF7 microcosms (Smooth, Large Smooth, Wrinkly Spreader, Small Disc, Large Disc), whereas A506 microcosms typically gave rise to two morphotype classes (Smooth, Web). Notably, the PICF7 wrinkly spreaders (WS) closely resemble the mat-forming WS morphotype of SBW25, and were seen arising from all 72-hr PICF7 microcosms. No wrinkly spreader colonies were observed arising from any of the 72-hr A506 microcosms. Further, none of the described emergent colony morphotypes were seen arising from 72-hr microcosms that were shaken (i.e., grown under conditions that preclude mat formation). Interestingly, however, A506 colonies from 72-hr shaken microcosms showed non-heritable variation in size. The mechanism behind this variation is unknown, but may be related to a frameshift mutation in A506 *rpoS*, resulting in non-functional RpoS and atypical regulation of the stress response (Hagen et al., 2009).

TABLE 1 A (non-exhaustive) list of genetic loci involved in exopolysaccharide production in SBW25, PICF7, and A506

Locus	Function	SBW25[a]	PICF7[b]	A506[c]
alg	Alginate biosynthesis	0979-0990	03390-03445	0959-0970
pel	Pel biosynthesis	–	06755-06785	–
pga	Pga biosynthesis	0143-0146	07400-07415	0154-0157
psl	Psl biosynthesis	2072-2082	26845-26895	1971-1982
wca	Colanic acid capsule biosynthesis	3655-3678	–	–
wss	Cellulose biosynthesis	0300-0309	–	–
aws	Regulation of EPS production	5209-5211	12635-12645	4497-4499
mwsR	Regulation of EPS production	5329	12125	4625
wsp	Regulation of EPS production	1219-1225	02220-02250	1184-1190

Note: Further details of selected loci are provided in Table S2. Synonyms include *awsXRO/tpbB/yfiBNR*; *mwsR/morA*.

[a]SBW25 genes are listed as PFLU locus tags.

[b]PICF7 genes are listed as PFLUOLIPICF7_RS locus tags.

[c]A506 genes are listed as PflA506 locus tags.

Although PICF7 and A506 form mats in 72-hr microcosms, these mats typically require 48–72 hr to fully develop. To test which, if any, of the emergent colony morphotypes had gained the ability to develop mats more quickly, examples of each morphotype were purified and inoculated into fresh microcosms. After only 24 hr, robust mats had formed in microcosms seeded by five of the ten morphotypes: SBW25 wrinkly spreader (SBW25-WS), PICF7 wrinkly spreader (PICF7-WS), PICF7 large smooth (PICF7-LSm), PICF7 small disc (PICF7-SD), and A506 web (A506-Web) (Figures 2c and S2).

The results in this section demonstrate that both PICF7 and A506 develop mats in 72-hr static microcosms, and that mat formation is accompanied by the emergence of new colony morphotypes. In PICF7, at least three morphotypes may contribute to the 72-hr mat (WS, LSm, SD), whereas the A506 mat is likely underpinned by the web morphotype. From this point forward, we characterize the molecular mechanisms underpinning mat formation in the emergent PICF7-WS and A506-Web morphotypes.

2.3 | PICF7 wrinkly spreaders carry mutations in *wsp*, *aws*, or *mwsR*

The mats (and WS colonies) observed from PICF7 72-hr static microcosms strongly resemble their SBW25 counterparts. In particular, they have the emergent property of developing a robust mat within 24 hr, and the wrinkly phenotype is heritably stable (i.e., when PICF7-WS colonies are sub-streaked on agar, they give rise to almost exclusively WS colonies). In order to determine whether the same mutational pathways underpin the WS phenotype in PICF7 and SBW25, ten WSs were isolated from independent, 72-hr microcosms founded by PICF7 (giving PICF7-WS1 to 10) and SBW25 (giving SBW25-WS1 to 10). Whole genome sequencing of these twenty WS genotypes revealed a mutation in *wsp*, *aws*, or *mwsR* in every case (Table 2 and Text S1). Six PICF7-WS types carried mutations in the *wsp* locus (vs. four SBW25-WSs), three in the *aws* locus (vs. two SBW25-WSs), and one in *mwsR* (vs. four SBW25-WSs). Each mutation is predicted to increase c-di-GMP production by WspR, AwsR, or MwsR, presumably leading to the activation of EPS biosynthesis and subsequent mat formation (see Text S1).

2.4 | The Pel polymer contributes to the structure of the PICF7 wrinkly spreader mat

Despite the phenotypic and genotypic similarities between PICF7-WS and SBW25-WS, the mats formed by each must differ on a structural level because PICF7 lacks homologues of the cellulose-biosynthetic *wss* genes that are activated by *wsp*, *aws*, or *mwsR* mutations in SBW25-WS. However, PICF7 carries several other polymer biosynthetic loci that could conceivably be activated by *wsp*, *aws*, or *mwsR* mutations (see Table 1). To investigate the structural basis of the PICF7-WS phenotype, a suppressor analysis was performed on PICF7-WS3, -WS4, -WS7, and -WS8 (carrying mutations in *wspF*, *awsX*, *mwsR*, and *wspF*, respectively). Each genotype was subjected to random transposon mutagenesis, and transposon mutants that had reverted to the smooth colony phenotype, and lost the ability to form 24-hr mats in static microcosms, were obtained. The genomic location of the transposon was determined in these mutants. Overall, approximately 15,600 transposon mutants were screened, and the insertion site determined in 100 suppressor mutants (Table S4).

Multiple independent transposon insertions were obtained in two types of loci. Firstly, 29 independent insertions were obtained in the *wsp*, *aws*, or *mwsR* loci. These insertions directly counteract the WS mutation in each background, presumably lowering c-di-GMP levels and ultimately reversing the WS phenotype. Secondly, 14 independent insertions were obtained in the seven-gene EPS biosynthetic locus, *pelA-G* (*PFLUOLIPICF7_RS06755-PFLUOLIPICF7_RS06785*; Figure 3a). It is probable that this class of suppressor mutants maintains high c-di-GMP levels, but loses the WS phenotype because the downstream EPS target (Pel) is inactivated. In three *pel* transposon mutants—carrying insertions in *pelA* (*PFLUOLIPICF7_RS06785*), *pelD* (*PFLUOLIPICF7_RS06770*), and *pelG* (*PFLUOLIPICF7_RS06755*)—a

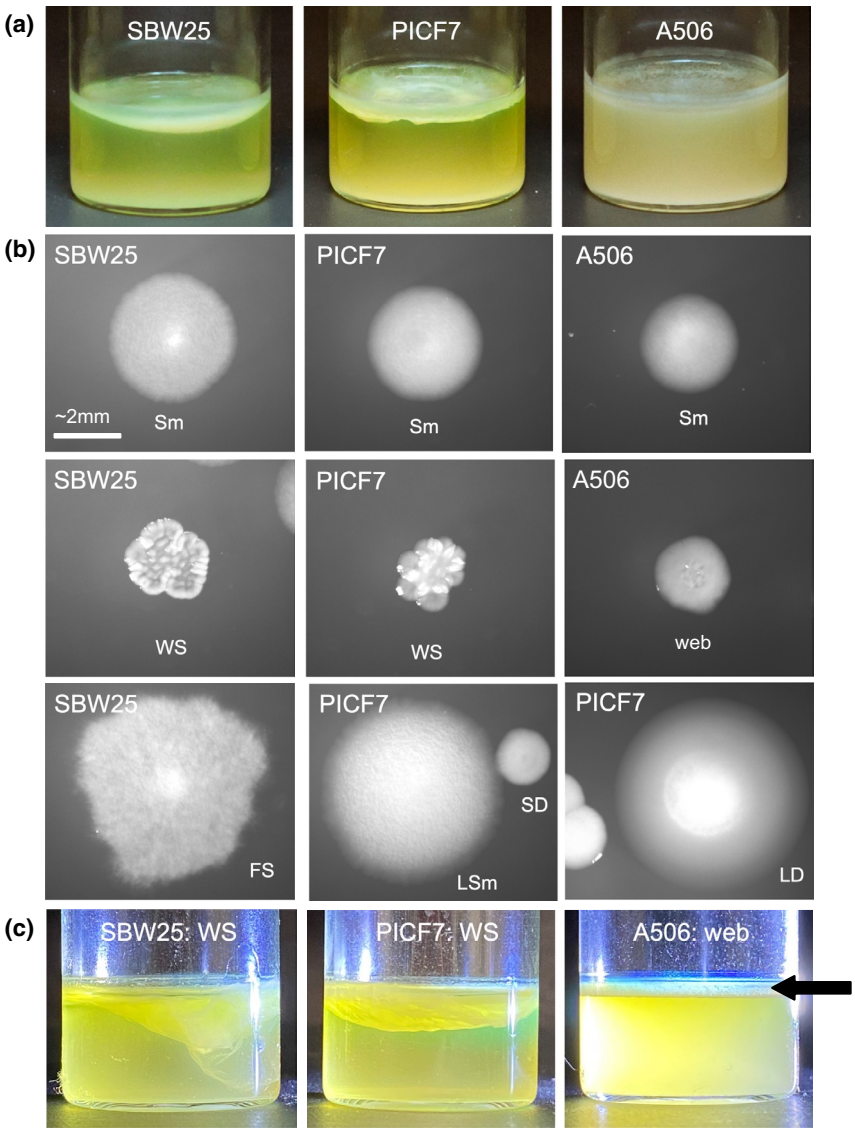

FIGURE 2 Mat formation and emergent colony diversity in PICF7 and A506 relative to SBW25. (a) Representative 72-hr microcosms founded by SBW25, PICF7, and A506. All three strains develop mats at the air-liquid interface within 72 hr. (b) Dilution plating from microcosms shows ten morphotypes: three in SBW25 (Smooth (Sm), Wrinkly Spreader (WS), Fuzzy Spreader (FS)), five in PICF7 (Smooth (Sm), Wrinkly Spreader (WS), Large Smooth (LSm), Large Disc (LD), and Small Disc (SD)), and two in A506 (Smooth (Sm), and Web). (c) SBW25-WS, PICF7-WS, and A506-Web give rise to mats at the air-liquid interface within 24 hr. The A506 mat is indicated by the black arrow. See Figure S2 for images of 24-hr microcosms from other morphotypes. Brightness and exposure of some images were altered in Preview

Cre-mediated recombination protocol was used to remove the majority of the transposon, leaving only a 189-bp scar at the insertion site and thereby eliminating possible polar effects. The Cre-deletion genotypes gave rise to smooth colonies and were unable to form robust 24-hr mats (Figure 3b,c), demonstrating that at least three of the seven *pel* genes are essential for the realization of the PICF7-WS phenotype. Preliminary investigations, in which a *pelA-lacZ* gene fusion was constructed, indicate that over-production of Pel in PICF7-WS is controlled—at least in part—at the level of *pel* transcription (Figure S3 and Text S3). We conclude that Pel is an important, c-di-GMP regulated, structural component of the PICF7-WS mat.

2.5 | The A506-Web colony phenotype is semi-heritable

In contrast to SBW25-WS and PICF7-WS, the A506-Web phenotype is only semi-heritable (i.e., unstable). That is, A506-Web colonies derived from 72-hr static microcosms rapidly and repeatedly gave rise to a mixture of web and smooth (i.e., wild-type-like) colonies when re-streaked on KB agar (Figure 4a). Further, when cells from A506-Web colonies were grown in shaken overnight culture (i.e., an environment that precludes mat formation) and plated on KB agar, between 9% and 45% of the resulting colonies reverted to the ancestral, smooth morphotype (Figure 4b and Table S5). No such colony diversity was observed arising from cells of mat-forming morphotypes A506-*wspF*-LoF, SBW25-WS, PICF7-WS, PICF7-LSm, or PICF7-SD (Figure 4b and/or Table S5). Of the web and smooth colony types arising from A506-Web, only the web type retained the ability to give rise to robust mats in 24-hr static microcosms (Figure 4c).

The relative ease with which the A506-Web phenotype reverts to the wild-type phenotype suggests that, unlike PICF7-WS and SBW25-WS, A506-Web is not underpinned by a stable genetic change. Indeed, no SNPs or indels were confirmed on the A506 chromosome or plasmid during whole genome re-sequencing of the 10 independent A506-Web isolates (Table S3). Interestingly, evidence of large-scale, tandem duplication events was found in

TABLE 2 Details of mutations identified in 10 wrinkly spreaders strains isolated from each of PICF7 and SBW25

Gene	Locus tag	Isolate number	Nucleotide change	Protein change	Ref[†]
PICF7-WS					
awsO	*PFLUOLIPICF7_RS12645*	6	t127a	F43I	
awsX	*PFLUOLIPICF7_RS12635*	4, 5	Δ232-264	Δ78-88 (ΔYTDDLIKGTTQ)	2–7
mwsR	*PFLUOLIPICF7_RS12125*	7	g2976t	M992I	
wspA	*PFLUOLIPICF7_RS02250*	1	c161t	S54L	
wspF	*PFLUOLIPICF7_RS02225*	2	c250t	R82(STOP)	
wspF	*PFLUOLIPICF7_RS02225*	3	c747g	I248(STOP)	
wspF	*PFLUOLIPICF7_RS02225*	8	a880c	T294P	
wspF	*PFLUOLIPICF7_RS02225*	9	Δ949-951	ΔA317	
wspF	*PFLUOLIPICF7_RS02225*	10	c898t	Q300(STOP)	
SBW25-WS					
awsR	*PFLU5210*	6	a79c	T27P	
awsR	*PFLU5210*	7	g574a	A192T	
mwsR	*PFLU5329*	1	g3244a	E1082K	
mwsR	*PFLU5329*	2	a2476t	S826C	
mwsR	*PFLU5329*	3	t2183c	V728A	
mwsR	*PFLU5329*	5	g3095t	R1032L	3
wspA	*PFLU1219*	9	c1313t	S438F	
wspE	*PFLU1223*	10	g1912t	D638Y	7
wspF	*PFLU1224*	4	Δ151-165	Δ51-55 (ΔLMDLI)	1
wspF	*PFLU1224*	8	Δ677-826	Δ226-275 (Δ50 residues)	6

[†]Reference is provided if a change in the same amino acid(s) has previously been reported to cause the wrinkly spreaders phenotype in *Pseudomonas fluorescens* SBW25. 1 = Bantinaki et al., 2007, 2 = Beaumont et al., 2009, 3 = Gallie et al., 2015, 4 = Gallie et al., 2019, 5 = Lind et al., 2017, 6 = Lind et al., 2019, 7 = McDonald et al., 2009. See Text S1 for further molecular details.

all ten A506-Web isolates, suggesting a flexible region of the chromosome to one side of the replication terminus (Text S2). The affected regions vary in size (~158 to ~634 kb) and precise location (between genomic positions 1,900,000 and 2,897,000 bp), but each contains a shared segment of ~126 kb beginning at genomic position ~2,314,000 bp. While intriguing, these amplifications are not thought to contribute to the web phenotype, because (i) a similar region was observed upon sequencing the A506 wild-type, and (ii) the set of ~118 genes encoded in the shared region does not include any genes with obvious roles in EPS synthesis or regulation (e.g., *aws*, *mwsR*, *pga*, *psl*, *wsp*) (Table S6).

2.6 | A deletion in *wspF* leads to a stable, web-like phenotype in A506

Even though *wsp/aws/mwsR* mutations were not identified in any of the ten A506-Web isolates, seemingly complete homologues of all three loci exist in A506 (Tables 1 and S2). This begs the question of whether mutations in these loci *could* generate differences in colony morphology, and the ability to form robust mats within 24 hr. To investigate, a scar-free, loss-of-function mutation was constructed in A506 *wspF* (Δ151-165 in *PflA506_1189*, leading to the deletion of amino acids 51–55; see Text S3). This mutation is a commonly occurring loss-of-function mutation underpinning the SBW25-WS phenotype (Bantinaki et al., 2007; Gallie et al., 2019; SBW25-WS4 of this study). The resulting genotype, A506-*wspF*-LoF, forms colonies that are similar in appearance to A506-Web colonies ("web-like"), and robust 24-hr mats (Figure 4a,c). Further, the web-like colony phenotype is stable; A506-*wspF*-LoF web-like colonies give rise to exclusively web-like colonies when streaked on agar plates, and when plated after growth in shaken overnight culture (Figure 4b).

A506 carries the genetic and molecular machinery required to produce mats by at least one of the same mutational routes as SBW25-WS and PICF7-WS (loss-of-function mutations in *wspF*). Despite this, mat formation by a readily reversible route is favored in 72-hr static microcosms founded by A506.

2.7 | Psl and Pga contribute to the A506-*wspF*-LoF web-like phenotype

The above section demonstrates that mutational inactivation of *wspF* in A506 leads to the ability to form robust mats within 24 hr. An attempt to identify the major structural component of this mat by random transposon mutagenesis was unsuccessful yet illuminating; fifteen A506-*wspF*-LoF suppressor mutants—each with smooth colony morphology and the inability to form robust 24-hr mats—were

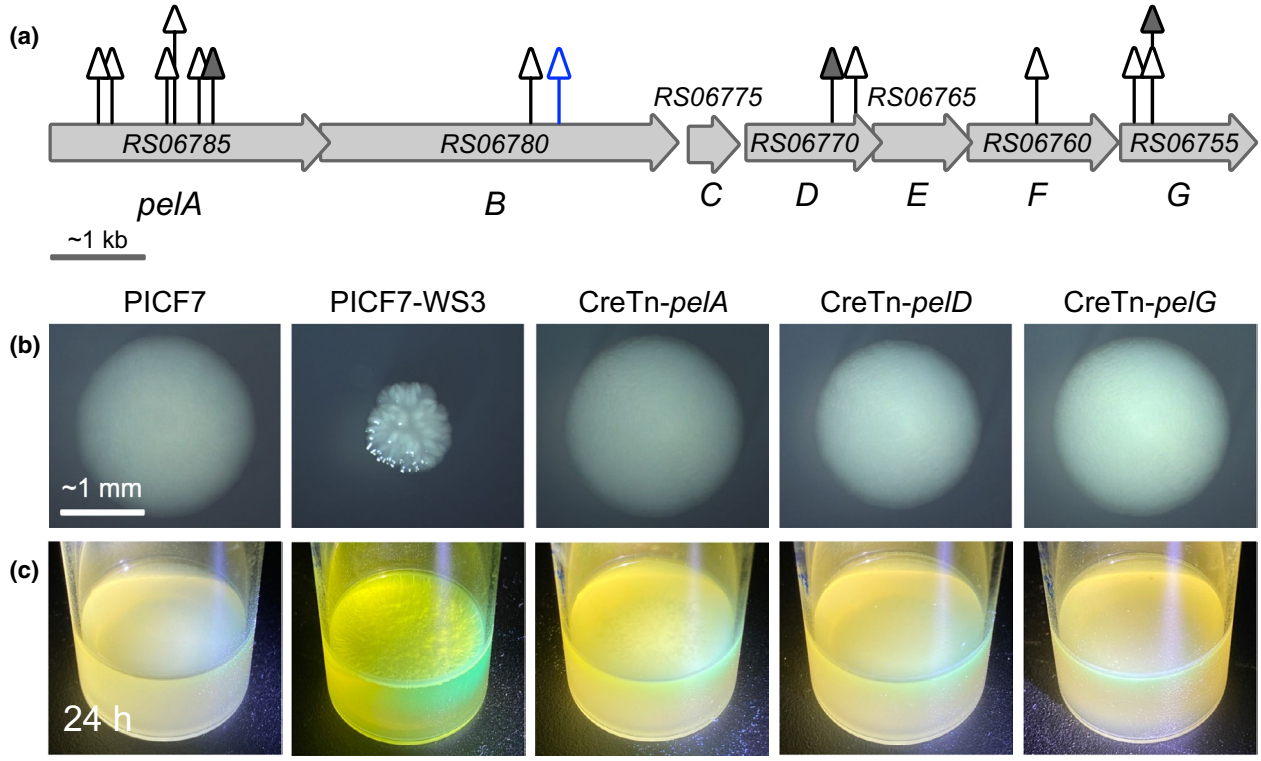

FIGURE 3 Pel is the major structural component of the PICF7-WS phenotype. (a) Fourteen independent WS suppressors were obtained in five out of seven genes of the PICF7 *pel* locus (*pelA-G*; Tables S2 and S4). Grey triangles = transposon mutants obtained in the background of a *wspF* mutation (PICF7-WS3, PICF7-WS8); blue triangle = transposon mutant obtained in the background of the *awsX* mutation (PICF7-WS4); open triangles = mutants carrying the full transposon; solid triangles = mutants in which a Cre-mediated deletion of the original transposon has been constructed (giving CreTn-*pelA*, CreTn-*pelD*, CreTn-*pelG*). The Cre-deleted transposon mutants have lost the WS colony morphology on KB agar (b), and no longer form robust mats in static microcosms within 24 hr (c). The exposures of some colony images were altered in Preview

found to contain insertions exclusively in the *wsp* operon (Table S4). The lack of insertions in polymer biosynthetic loci—or indeed, any loci other than *wsp*—is notable, and suggests that multiple EPSs may contribute to the web-like phenotype of A506-*wspF*-LoF (i.e., inactivating insertions in any individual EPS biosynthetic loci would not be expected to entirely restore smooth colony morphology).

There are at least three candidate polymers that could conceivably contribute to mat formation by A506-*wspF*-LoF: Psl, Pga, and alginate (see Table 1). Of these, Psl and Pga have been shown to be regulated by c-di-GMP in other pseudomonads (Borlee et al., 2010; Lind et al., 2017; Malone et al., 2010). To directly test the roles of Psl and Pga in A506-*wspF*-LoF mat formation, the eleven-gene *psl* operon (*pslA-K*; *PflA506_1971* to *PflA506_1982*) and four-gene *pga* operon (*pgaA-D*; *PflA506_0154* to *PflA506_0157*) were deleted from A506-*wspF*-LoF, separately and in combination (giving A506-wspF-LoF-Δ*psl*, -Δ*pga*, and -Δ*psl*Δ*pga*; see Text S3). The effects of Psl and/or Pga elimination on A506-*wspF*-LoF colony morphology (Figure 5a) and mat formation (Figure 5b–d) were examined.

Although the elimination of neither Psl nor Pga alone significantly affected A506-*wspF*-LoF colony morphology, their simultaneous elimination resulted in loss of web-like colony morphology. Notably, even the double deletion did not entirely restore smooth colony morphology; A506-*wspF*-LoF-Δ*psl*Δ*pga* gives rise to slightly shiny colonies with concentric circles ("Disc" colonies in Figure 5a). These observations are consistent with the lack of single-locus transposon insertions identified in polymer biosynthetic loci in the A506-*wspF*-LoF suppressor analysis (see Table S4); simultaneous inactivation of *psl* and *pga* is required to see an appreciable change in A506-*wspF*-LoF colony morphology.

Despite the lack of effect on web-like colony morphology, deletion of *psl* alone severely impeded mat formation by A506-*wspF*-LoF; A506-*wspF*-LoF-Δ*psl* forms substantially less robust mats at 24, 48, and 72 hr than does A506-*wspF*-LoF (Figure 5b–d). The elimination of Pga had a far more subtle effect on mat formation; microcosms founded with A506-*wspF*-LoF-Δ*pga* generally formed a robust mat within 72 hr, but often required longer than A506-*wspF*-LoF to do so. Simultaneous elimination of Psl and Pga resulted in the inability to form any sort of mat within 24 hr (and only a very fragile, partial mat within 72 hr) (Figure 5b–d).

The work in this section demonstrates that both Psl and Pga contribute to the web-like phenotype of A506-*wspF*-LoF. Presumably, hyperactivity of WspR—caused by mutational inactivation of *wspF*—stimulates the expression and/or downstream activity of the Psl and Pga biosynthetic pathways, leading to the web-like colony morphology and rapid mat formation. Hence, the Wsp chemosensory pathway regulates the production of different EPSs in each of our three

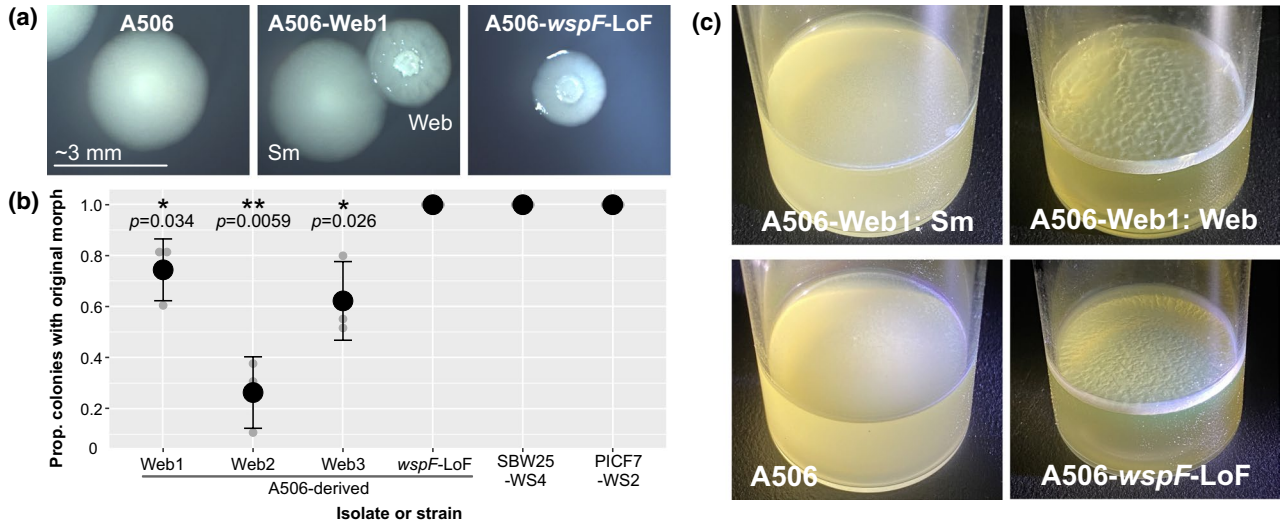

FIGURE 4 Semi-heritable (A506-Web) and heritable (A506-*wspF*-LoF) routes to mat formation in A506. (a) A506-Web isolates from 72-hr static microcosms give rise to a mixture of smooth (Sm) and web colonies on KB agar (A506-Web1 is pictured as an example). A506-*wspF*-LoF, carrying a loss-of-function mutation in *wspF*, consistently generates colonies with a similar, web-like appearance. (b) A stability assay demonstrates significant loss of the web morphotype in colonies plated from shaken overnight cultures of A506-Web (one-tailed, one sample *t*-tests $p < .034$; see also Table S5), no loss of the web-like morphotype in A506-*wspF*-LoF, and no loss of the WS morphotype in SBW25-WS4 or PICF7-WS2 (both carrying loss-of-function *wspF* mutations). Three biological replicates were performed for each strain, with a minimum of 45 colonies counted across three plates per replicate. Grey dots are individual data points, black dots are means, and black whiskers are standard errors (see Table S5). (c) Like A506, smooth colonies isolated from A506-Web1 in panel A (A506-Web1:Sm) do not develop robust mats in 24-hr static microcosms. Both web colony counterparts (A506-Web1:Web and A506-*wspF*-LoF) form robust mats within 24 hr. Exposures of some colony images were altered in Preview

pseudomonads: (i) cellulose in SBW25, (ii) Pel in PICF7, and (iii) Psl/Pga in A506.

2.8 | Psl and Pga contribute to A506 mat formation

Work thus far demonstrates that Psl and Pga contribute to robust 24-hr mat formation in the presence of mutations that constitutively activate the Wsp chemosensory pathway. Whether these EPSs play a similar role in the production of robust 24-hr mats by the A506-Web morphotype—in which no mutations, *wspF* or otherwise, have been identified—remains unclear. This question cannot be addressed simply by deleting *psl* and/or *pga* from A506-Web, due to the rapidity with which A506-Web reverts to the smooth morphotype (see Figure 4). Therefore, *psl* and *pga* were deleted separately and in combination from wild-type A506 (giving A506-Δ*psl*, -Δ*pga*, and -Δ*psl*Δ*pga*; see Text S3), and the effects on colony morphology and mat development observed (Figure 6).

Elimination of Psl and/or Pga had no readily discernible effects on A506 colony morphology (Figure 6a), but affected mat formation in various ways (Figure 6b–d). Firstly, Psl elimination resulted in (i) loss of the ability to form a weak mat within 24 hr (see also first results section), and (ii) the formation of 48–72 hr mats that were morphologically distinct from those of wild-type A506. These observations show that Psl plays a central role in colonization of the air-liquid interface by A506, but mat formation can nevertheless still be achieved by alternative routes. As in the A506-*wspF*-LoF background (see Figure 5b–d), deletion of *pga* led to less obvious effects on mat formation; microcosms founded with A506-Δ*pga* tended to form mats more slowly—and with a subtly different morphology—compared to those founded by A506 (Figure 6b–d). Deletion of both *psl* and *pga* perturbed mat formation at 24, 48 and 72 hr (Figure 6b–d). Further, deletion of *psl* and *pga* impeded the emergence of the web morphotype: no A506-Web colonies were seen when plating from five replicate 72-hr microcosms founded by A506-Δ*psl*Δ*pga*. Instead, a different emergent colony type—strongly resembling the Disc colonies produced by A506-*wspF*-LoF-Δ*psl*Δ*pga* (see Figure 5a)—was observed (Figure 6e). Each of five control microcosms founded by A506 gave rise to A506-Web colonies and no Disc colonies.

As in A506-*wspF*-LoF background, Psl and—to a lesser extent—Pga are important structural components in the formation of mats by A506 wild-type. Elimination of both EPSs in A506 disrupts the ability to colonize the air-liquid interface, and impedes the emergence of the unstable A506-Web morphotype.

3 | DISCUSSION

P. fluorescens SBW25 readily forms robust mats at the air-liquid interface of 72-hr static microcosms. These mats result from mutations that elevate the c-di-GMP output of WspR, AwsR, or MwsR, leading to the production of cellulose and/or Pga and the wrinkly spreader phenotype (Bantinaki et al., 2007; Lind et al., 2017, 2019; McDonald et al., 2009; Rainey & Travisano, 1998). Here, we have investigated the divergent mechanisms by which SBW25 relatives

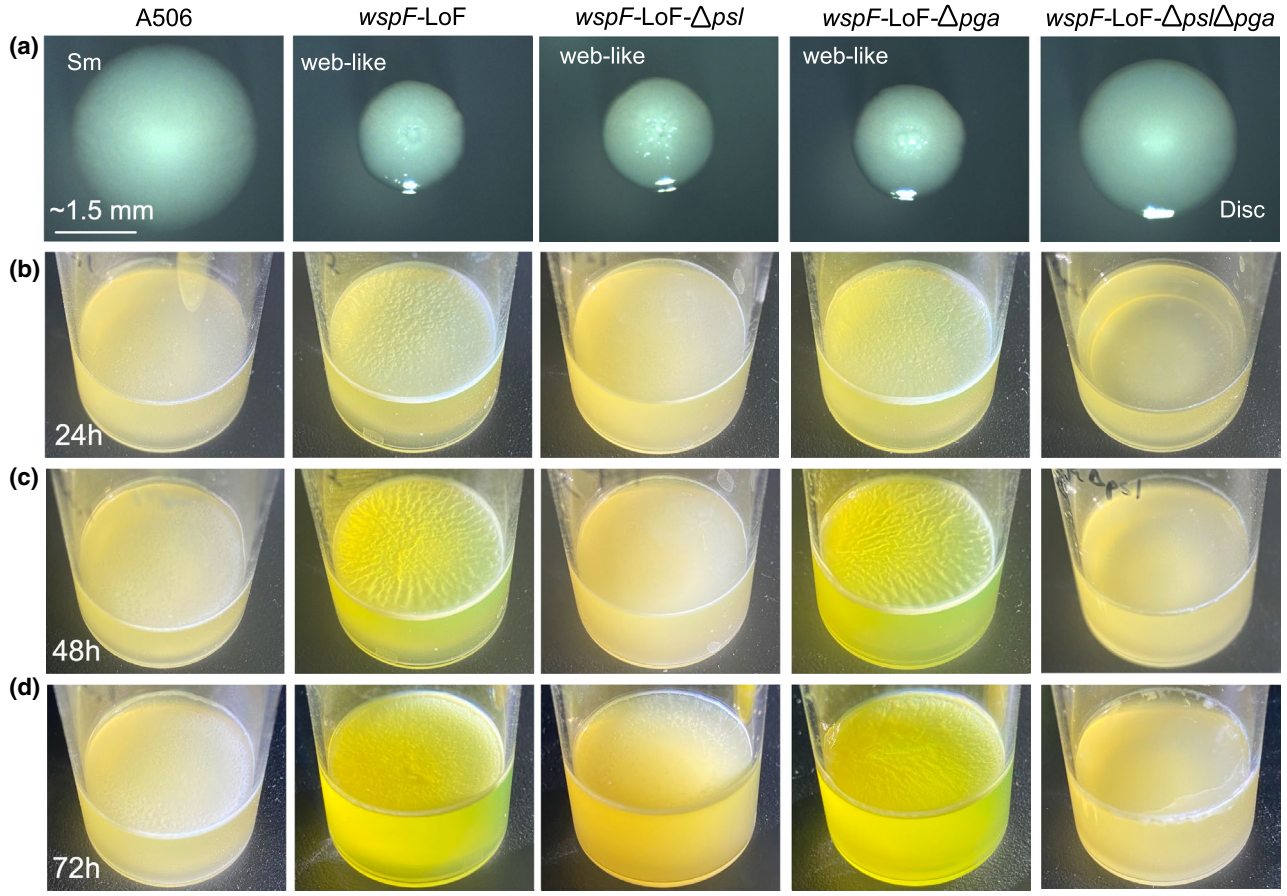

FIGURE 5 Psl and Pga contribute to the A506-*wspF*-LoF web-like phenotype. (a) Simultaneous deletion of the *psl* and *pga* loci visibly affects the web-like colony morphology of A506-*wspF*-LoF. Colonies were grown on KB agar for 48 hr. Scale bar applies to all images. Exposures of colony images were altered in Preview to increase visibility. (b–d) Deletion of *psl* and, to a lesser extent, *pga* impairs A506-*wspF*-LoF mat formation at the air-liquid interface of static microcosms

P. simiae PICF7 and *P. fluorescens* A506 produce 72-hr mats. The details of mat formation in PICF7 and A506 are discussed below, and a summary model is provided in Figure 7.

3.1 | A model for mat formation by PICF7-WS

One morphotype that contributes to the development of robust 72-hr mats in microcosms founded by PICF7 is the wrinkly spreader (PICF7-WS). There are notable parallels between PICF7-WS and SBW25-WS. In particular, (i) both WS types produce similar, heritably stable, wrinkly colonies and robust 24-hr mats, and (ii) these phenotypes are underpinned by c-di-GMP-elevating mutations in *wsp*, *aws*, or *mwsR* homologues. However, the downstream targets of c-di-GMP differ in the two backgrounds. In SBW25, elevated c-di-GMP stimulates cellulose production by the Wss biosynthetic machinery (Gal et al., 2003; Goymer et al., 2006; Spiers et al., 2002). PICF7 lacks *wss* homologues, and cannot synthesize cellulose. Instead, PICF7-WS requires the production of Pel (Figure 7).

Pel is a cationic, glucose-rich EPS that has mainly been characterized as a structural component of *P. aeruginosa* biofilms (Friedman & Kolter, 2004; Jennings et al., 2015). In *P. aeruginosa*, c-di-GMP-mediated production of Pel is required for the emergence of WS-like, rugose small-colony variants (RSCVs) (D'Argenio et al., 2002; Hickman et al., 2005; Starkey et al., 2009). C-di-GMP-mediated regulation of *P. aeruginosa* Pel production occurs through FleQ, a c-di-GMP binding transcriptional regulator. FleQ binds to two stretches of DNA upstream of *pelA*, and, in the absence of c-di-GMP, represses *pel* transcription (Hickman & Harwood, 2008). When DNA-bound FleQ interacts with c-di-GMP, the conformation of the region changes such that FleQ becomes a transcriptional activator of *pel* (Baraquet et al., 2012; Matsuyama et al., 2016). FleQ is also involved in c-di-GMP-dependent EPS production in *Pseudomonas putida* (Molina-Henares et al., 2017; Ramos-González et al., 2016).

The above suggests that FleQ may play a role in the c-di-GMP-mediated regulation of Pel production in PICF7. Indeed, a recent study reported that a PICF7 strain carrying an inactivating insertion in *fleQ* (PFLUOLIPICF7_16515) showed altered capacity to form a biofilm (Montes-Osuna et al., 2021). The extent to which, and mechanisms whereby, *fleQ* and other regulators are involved in PICF7 Pel regulation remain to be elucidated.

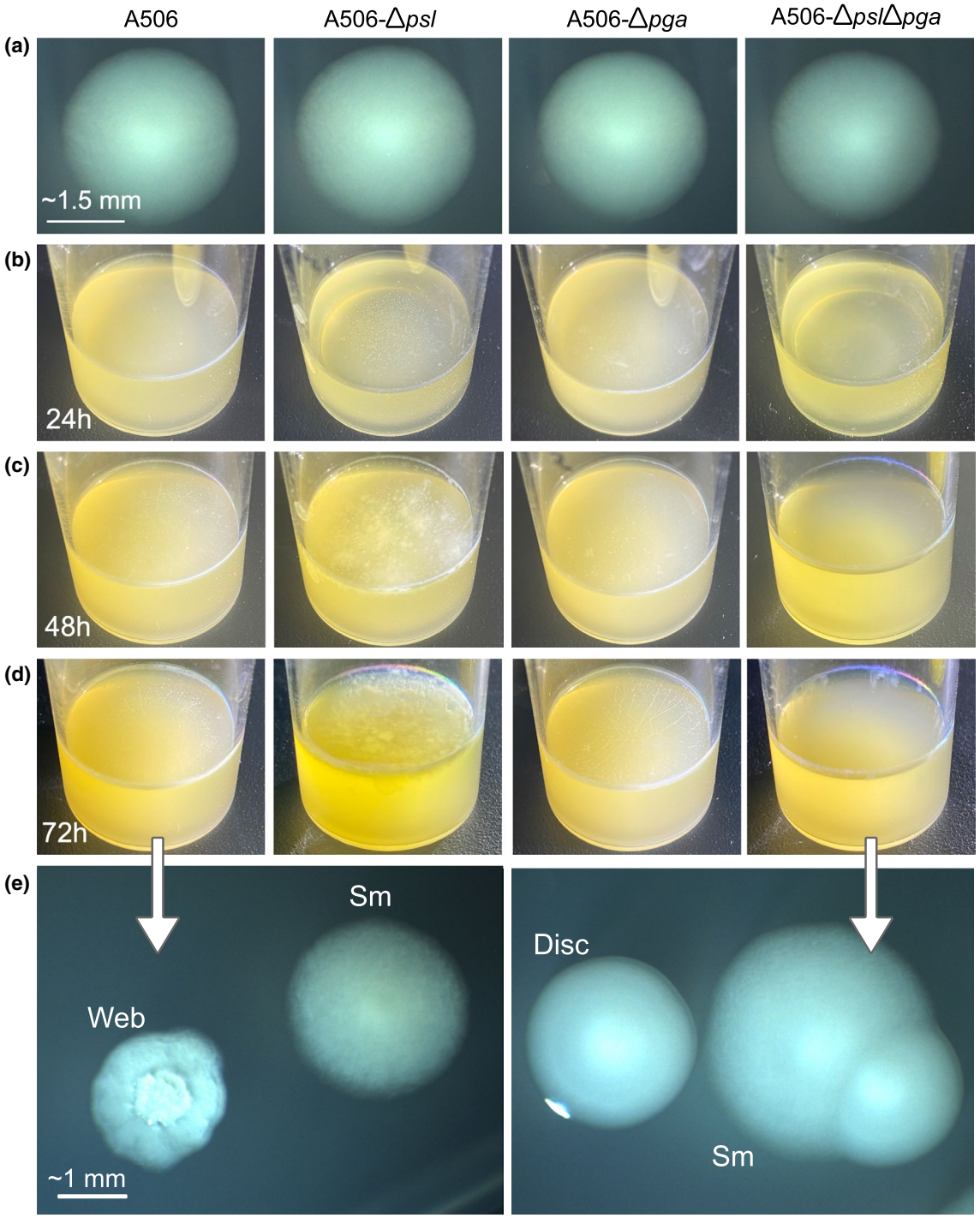

FIGURE 6 Psl and Pga contribute to mat formation by A506 wild-type. (a) Deletion of the *psl* and *pga* loci does not noticeably affect A506 colony morphology on KB agar (28°C, 48 hr). Scale bar applies to all images in this row. (b–d) Deletion of *psl*, *pga*, or both *psl* and *pga* affects A506 mat formation at 24, 48, and 72 hr. (e) Colony morphotypes derived from 72-hr static microcosms founded by A506 (left) or A506-Δ*psl*Δ*pga* (right). Colonies were grown on KB agar (28°C, 28 hr). Scale bar applies to both images. Exposures of colony images in (a) and (e) were altered in Preview to increase visibility

3.2 | Additional routes to mat formation in PICF7

In addition to WS, 72-hr PICF7 microcosms were typically observed to contain multiple other emergent colony morphotypes (LSm, SD, LD). Each morphotype has its own distinguishing phenotypic features, which presumably result from different molecular processes. With the exception of WS, these molecular processes remain almost entirely uncharacterized; they may or may not involve c-di-GMP, and may each regulate the expression of different downstream EPSs or cell surface components. We do know that at least three of the emergent morphotype classes—WS, LSm, and SD—appear to be heritable (i.e., are likely underpinned by stable mutations) (see Table S5).

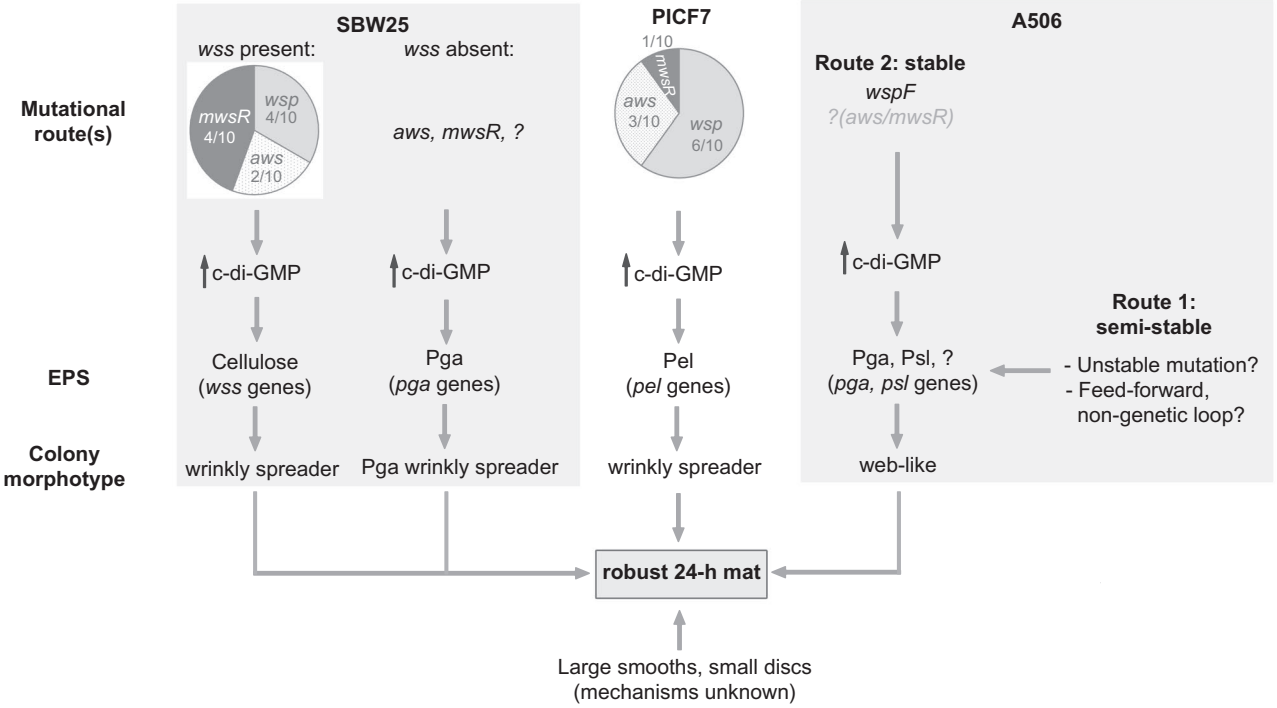

FIGURE 7 Model of the molecular routes to robust 24-hr mat formation in *Pseudomonas simiae* PICF7 and *Pseudomonas fluorescens* A506, as compared with the previously well-studied *P. fluorescens* SBW25. Pie charts were drawn using mutations identified by genome sequencing of ten WS genotypes in each of the SBW25 and PICF7 backgrounds (see Table 2)

In addition, these three morphotypes can independently form a 24-hr mat (see Figure S2), suggesting that each type arises and competes for dominance during development of the 72-hr PICF7 mat (and beyond; see Figure S1). The relative proportions of each morphotype have not yet been studied, but these are likely to depend on a combination of the rate at which each morphotype arises (e.g., mutational target size and localized mutation rates), and the relative fitness of each type in the emerging population.

The co-emergence of multiple, distinct mat-forming morphotypes strongly suggests that 72-hr PICF7 mats consist of phenotypically and genotypically heterogeneous subpopulations, possibly with each morphotype producing distinct EPSs, and/or cell surface components. PICF7 has the genetic capacity to produce several EPSs (including Pel, Pga, Psl, and alginate), and various cell surface components (e.g., adhesins, lipopolysaccharides, and pili). Expression of each of these components is expected to confer specific physicochemical properties on the surrounding cells (reviewed in Rehm, 2010), some of which may be beneficial in the natural plant environment.

3.3 | Molecular routes to semi-heritable mat formation by A506-Web

The formation of A506 mats over 72 hr is underpinned by the semi-heritable A506-Web morphotype, which forms colonies with a web-like internal structure that can form full mats within 24 hr. The A506-Web phenotype is less stable than the mat-forming morphotypes arising from 72-hr PICF7 and SBW25 microcosms. The degree of morphotype stability provides some insight into the underlying molecular causes of the phenotype. At one end of the scale, a readily reversible phenotype is likely to be underpinned by non-heritable mechanisms (e.g., activation of an EPS transcription factor in the presence of a particular environmental stimulus; see introduction). Such mechanisms can be switched on and off within the lifetime of a cell, and are thus not heritable. At the opposite end of the scale, an (almost) irreversible phenotype is likely to be underpinned by a stable genetic change (e.g., a deletion in *wspF* giving rise to the WS phenotype). In the absence of further mutation(s), the resulting phenotype is stable and heritable. The semi-heritable A506-Web phenotype is not expected to result from either a straightforward transcriptional change (no heritability), or a stable genetic change (heritability), but a mechanism that generates semi-heritability.

We see two hypothetical possibilities for a mechanism underpinning semi-heritability (Figure 7). Firstly, the A506-Web phenotype could conceivably result from a non-stable genetic change that flips between two states at relatively high frequency (i.e., phase variation). These types of mutations—examples of which include slippage in homopolymeric tracts (De Bolle et al., 2000; Orsi et al., 2010), site-specific inversions (Abraham et al., 1985; Dybvig & Yu, 1994), and tandem duplication events (Anderson & Roth, 1981; Ayan et al., 2020)—occur and revert randomly, but at frequencies several orders of magnitude higher than standard SNPs (reviewed in Anderson & Roth, 1977; Moxon et al., 2006). If such a high-frequency mutational locus were to exist within, for example, an A506 EPS biosynthetic locus, an initially clonal, growing population would rapidly

and repeatedly generate sub-populations of "EPS on" (web) and "EPS off" (wild-type). Once both forms exist, selection would act to influence the relative proportion of each form, with web and wild-type dominating in static and shaken environments, respectively. Although we did not find evidence of mutable loci underpinning the unstable A506-Web phenotype, we note that many kinds of high-frequency mutations are notoriously difficult to identify using whole genome resequencing. However, the rate at which the A506-Web morphotype reverted to the wild-type morphotype in overnight shaken culture was observed to be much higher than would typically be expected for phase variants (Anderson & Roth, 1977; Moxon et al., 2006).

A second possibility is that no genetic change is required to switch between A506-Web and wild-type morphotypes. Instead, semi-heritability may be achieved by a molecular network topology that can generate two distinct, semi-stable phenotypic states ("EPS on" or "EPS off") (Tiwari et al., 2011). To illustrate, imagine the following example. In the static microcosm, a signal activates expression of a transcription factor (TF), which in turn activates the transcription of (i) a DGC and/or EPS biosynthetic genes, and (ii) itself. This leads to (i) the "EPS on" state and mat formation, and (ii) self-perpetuating TF production that can persist even after the initial environmental stimulus is removed. A switch back to the "EPS off" state requires TF levels to stochastically drop below a particular threshold, perhaps as a result of stochastic division of intracellular protein content upon cell division. Examples of bistable molecular networks have been shown to underpin semi-heritable, ON/OFF expression of colanic acid-like capsules in *P. fluorescens* SBW25 (Gallie et al., 2015, 2019; Remigi et al., 2019), bistable expression of the PDE PdeL in *E. coli* (Reinders et al., 2016), and bistable white-opaque switching in *Candida albicans* (Zordan et al., 2006). Some bistable switches can switch between states more rapidly than is achieved by phase variation (e.g., Gallie et al., 2015; Remigi et al., 2019), and hence could conceivably be involved in the A506-Web phenotype.

The existence of a semi-heritable mechanism underpinning A506 mat formation provides a degree of phenotypic and evolutionary flexibility for A506 that has—at least so far—not been observed in laboratory populations of SBW25 and PICF7. Such a mechanism may enable A506 to amplify a stimulus, enabling ready and repeated switching between planktonic and sessile lifestyles, without the accumulation of irreversible, loss-of-function mutations in EPS biosynthetic pathways.

3.4 | A stable route to A506 mat formation: *wspF* mutations

In addition to the semi-heritable route, A506 can form stable, web-like colonies and robust 24-hr mats through at least one of the three mutational routes that underpin the SBW25-WS and PICF7-WS phenotypes: loss-of-function mutations in *wspF*, a negative regulator of the WspR DGC (Figure 7). Protein domain predictions for the Wsp pathway (see Table S2) are consistent with *wspF* mutations having similar downstream effects in all three strains: de-repression of WspR DGC activity, leading to an increase in c-di-GMP, and the production of at least one EPS (cellulose in SBW25, Pel in PICF7, and Psl/Pga in A506). Wsp-mediated control of these distinct EPSs demonstrates a degree of evolutionary flexibility in the major structural components of mats, indicating that EPS biosynthetic loci can be lost or gained, with seamless incorporation into existing host regulatory networks.

It is not entirely clear to what extent the web-like phenotype generated by mutation of *wspF* resembles the semi-heritable A506-Web phenotype (particularly at the molecular level). However, although many mutational routes to mat formation are presumably available in A506 (i.e., many loss of function mutations in *wspF*), our results indicate that genotypes carrying these mutations do not dominate in 72-hr A506 mats; all ten of our independently-isolated A506-Web types showed the semi-heritable web phenotype, and no *wspF* (or other) mutations were identified. The bias towards the semi-heritable route to mat formation may result from a higher rate of A506-Web generation than *wspF* mutation, and/or a selective advantage of A506-Web over *wspF* mutants.

The diversity of molecular and structural routes to mat formation in *P. fluorescens* SBW25, *P. simiae* PICF7, and *P. fluorescens* A506 demonstrates a high degree of evolutionary flexibility in EPS regulation, highlighting the ecological and evolutionary importance of mat formation.

4 | EXPERIMENTAL PROCEDURES

4.1 | Phylogenetic tree construction

The complete genome sequences of ten closely related *Pseudomonas* strains were downloaded from NCBI in February 2021 (for reference numbers see Table S1). Using REALPHY (version 1.13; Bertels et al., 2014) three whole-genome alignments were generated, in each of which the remaining nine genomes were aligned to the SBW25, A506, or RE*1-1-14 reference sequences, respectively. REALPHY merged the resulting three alignments into a single alignment consisting of 1,464,229 alignment columns. From this, a maximum likelihood tree was generated with PHYML (GTR substitution model, 100 bootstrap replicates) (Guindon & Gascuel, 2003), and visualized in Geneious (version 11.1.4) (Figure 1). The most divergent of strain, *P. fluorescens* UK4, was used as an outgroup to root the tree.

4.2 | Strains, plasmids, and oligonucleotides

Details of all strains, plasmids, and oligonucleotides used in this study are provided in Table S1.

4.3 | Growth conditions

Strains were grown in Lysogeny Broth (LB) or King's Medium B (KB; King et al., 1954), using the following recipes. LB: 10 g/L tryptone,

10 g/L NaCl, 5 g/L yeast extract, 15 g/L agar (for agar plates). KB: 20 g/L Proteose Peptone No.3 (Condalab, 1607; for liquid medium) or tryptone (Sigma-Aldrich T7293; for agar plates), 10 ml/L glycerol, 1.5 g/L $MgSO_4.7H_2O$, 1.95 g/L $K_2HPO_4.3H_2O$, 15 g/L agar (for agar plates). *Pseudomonas* strains were grown in KB at 28°C in static microcosms (see below), liquid culture (~18 hr, with shaking), or on agar plates (~48 hr). During cloning procedures, *E. coli* and *Pseudomonas* strains were grown in LB media at 37 and 28°C, respectively. Where appropriate LB was supplemented with nitrofurantoin (NF; 100 μg/ml), kanamycin (Km; 50 μg/ml), tetracycline (Tc; 12.5 μg/ml for *E. coli* and PICF7, 50 μg/ml for A506), and/or 5-Bromo-4-Chloro-3-Indolyl β-D-Galactopyranoside (X-gal; 60 μg/ml).

4.4 | Mat formation in static microcosms

Standard static microcosms were 30 ml glass tubes containing 6 ml liquid KB. Each microcosm was inoculated with 6 μl of stationary phase *Pseudomonas* culture, vortexed for 5 s, the lid loosened, and grown without agitation at 28°C for 24, 48 or 72 hr. To observe emergent colony morphotypes, lids were tightened, the microcosms vortexed for 1 min, serially diluted in Ringer's Solution, and plated on KB agar (28°C, 48 hr).

4.5 | Photography

Colonies were visualized under a Leica MS5 dissection microscope, and photographed with a VisiCam® 1.3 (VWR International). Microcosm photographs were taken with an iPhone 11. Photographs were cropped and, where noted in figure legends, the exposure and/or brightness uniformly altered in Preview (v11.0) to improve visibility.

4.6 | Whole genome sequencing

Single colony isolates were grown to stationary phase in liquid KB (shaking) and genomic DNA isolated with a Qiagen DNeasy Blood and Tissue Kit (Qiagen). Extracted genomic DNA was checked for quality using agarose gel electrophoresis and a Nanodrop™ 3300 Fluorospectrometer. Whole genome re-sequencing was subsequently performed by the sequencing facility at the Max Planck Institute for Evolutionary Biology (Ploen, Germany), in three separate runs. The first run aimed to identify mutations in 30 SBW25-WS, PICF7-WS, and A506-Web isolates. 300 bp, paired-end reads were generated with a MiSeq Reagent Kit v3 (Illumina). Usable data was generated for 29 of 30 isolates; PICF7-WS5 was unsuccessful. PICF7-WS5 was re-sequenced in a second run, during which 150 bp, paired-end reads were generated with a NextSeq 550 Output v2.5 Kit (Illumina). A third run was used to generate high coverage reads for A506 wild-type and one A506-Web isolate (A506-Web5). 150 bp, paired-end reads were generated with a NextSeq 550 Output v2.5 kit (Illumina). All sequencing reads are available at NCBI Sequence Read Archive (Leinonen et al., 2011), under BioProject number PRJNA730882.

4.7 | Analysis of whole genome sequencing data for PICF7-WS and SBW25-WS

A minimum of 1 million reads per isolate were aligned to the PICF7 (GenBank CP005975.1; Martínez-García et al., 2015) or SBW25 (RefSeq NC_012660.1; Silby et al., 2009) reference genome sequences, using *breseq* (Barrick et al., 2014; Deatherage & Barrick, 2014). A minimum mean coverage of 26.3 and 28.9 was obtained for the PICF7-WS and SBW25-WS genotypes, respectively. A list of possible mutations was generated for each genome (Table S3), and unique mutations were confirmed in the genome of interest by PCR amplification and Sanger sequencing. In isolates where no unique candidate mutations were initially identified by *breseq* (SBW25-WS6 and SBW25-WS8), WS mutations were identified by PCR amplification and Sanger sequencing of commonly mutated loci in WS types. See Text S1 for a detailed description of WS mutations.

4.8 | Analysis of whole genome sequencing data for A506 and A506-Web

The first attempt at re-sequencing A506-Web isolates resulted in the prediction of >200 mutations per isolate by *breseq*, many of which were present in all ten isolates (Table S3). To clarify which, if any, of these predicted mutations were real and relevant to the Web phenotype, we sequenced our copy of A506 wild-type and one Web isolate (A506-Web5) at high coverage. For each of these two samples, slightly under 6 million 150 bp, paired-end sequencing reads were obtained, and aligned to the NCBI reference sequences for the A506 chromosome (NC_017911.1; Loper et al., 2012) and plasmid (NC_021361.1; Stockwell et al., 2013) using *breseq* (Barrick et al., 2014; Deatherage & Barrick, 2014). Mean coverages of 144.9 and 139.9 (A506 wild-type chromosome and plasmid, respectively), and 151.1 and 111.9 (A506-Web5 chromosome and plasmid, respectively) were obtained, and ~100 mutations were predicted in each sample. All differences predicted in A506-Web5 were also predicted in A506 wild-type, and no convincing additional differences were found in the lower coverage genome re-sequencing in any of the other Web isolates (Table S3).

4.9 | Transposon mutagenesis

Four *P. fluorescens* PICF7 WS genotypes (-WS3, -WS4, -WS7, -WS8; carrying mutations in *wspF*, *awsX*, *mwsR*, *wspF*, respectively) and A506-*wspF*-LoF (carrying *wspF* mutation Δ151-165)

were subjected to a suppressor analysis via random mutagenesis with the IS-Ω-Km/hah transposon (Jacobs et al., 2003). The protocol previously described for the mutagenesis of *P. fluorescens* SBW25 (Giddens et al., 2007) was used, with the exception that the recipient genotypes were not subjected to a heat shock prior to biparental conjugation. For PICF7-WS strains, approximately 15,600 transformant colonies from eleven independent conjugations were screened for loss of the WS colony phenotype. For A506-*wspF*-LoF, approximately 2,300 transformant colonies from two conjugations were screened for loss of the web-like colony phenotype. Both sets of isolated mutants were then screened for loss of the ability to form robust, 24-hr mats. The transposon insertion site was determined in 100 PICF7-WS suppressor mutants and 15 A506-*wspF*-LoF suppressor mutants (Table S4). In selected PICF7-WS suppressor mutants, the bulk of the IS-Ω-Km/hah transposon was deleted using Cre-*loxP*-mediated recombination; the pCre vector (Manoil, 2000) was transiently introduced into transposon mutants of interest, and colonies that had lost the Km resistance conferred by the transposon ("CreTn" types) were isolated. This process leaves a 189-bp scar that disrupts the function of the gene in which the insertion occurs without affecting the expression of downstream genes or operons (i.e., produces a non-polar mutation; Giddens et al., 2007).

4.10 | Colony morphotype stability test

Single colonies of six strains (A506-Web1, A506-Web2, A506-Web3, A506-*wspF*-LoF, SBW25-WS4, and PICF7-WS2) were grown from glycerol stocks on KB agar (28°C, 48 hr). For each strain, three single colonies displaying the Web or WS phenotype were grown overnight in shaken liquid KB (28°C, 200 rpm). Overnight cultures were vortexed, dilution plated on KB agar, and incubated at 28°C for 48 hr. For each culture, between 45 and 300 colonies were observed, across at least three KB plates. The proportion of colonies showing the original morphotype (Web, WS) was recorded, and the mean and standard error of the proportion of cells in each culture carrying calculated (Figure 4b and Table S5). Parametric, one-tailed, one-sample *t*-tests were used to detect loss of Web colony morphology in A506-Web types. In the case of strains carrying a *wspF* mutation (A506-*wspF*-LoF, SBW25-WS4, PICF7-WS2), no variation in colony morphology was observed. Analyses were performed in R (v3.6.0). Significance levels $^{*}.05 < p < .01$, $^{**}.01 < p < .001$, and all *p*-values in the main text are reported to 2 s.f. A similar, smaller-scale assay was subsequently performed as a preliminary test of PICF7-LSm and PICF7-SD morphotype stability (Table S5).

4.11 | Genetic engineering in A506

Scar-free deletions were constructed in A506 using a similar protocol to that outlined for SBW25 (Zhang & Rainey, 2007). Briefly, deletion fragments were constructed by SOE-PCR (Ho et al., 1989), ligated into the suicide vector pUIC3 (Rainey, 1999), and delivered into the relevant A506 background using a recombination-based, two-step allelic exchange protocol. The differences to the SBW25 protocol are as follows: (i) A506 was not subjected to a heat shock prior to the first recombination event, (ii) a higher concentration of Tc (50 μg/ml) was used to select first recombinants, and (iii) cycloserine enrichment was not used to enrich for second recombinants; first recombinant types were simply grown in flasks and plated onto LB+X-gal agar to identify colonies that had lost the pUIC3 vector (i.e., white, Tc sensitive colonies). Presence of the deletion was confirmed using PCR and Sanger sequencing with primers outside the manipulation region. In each case, the final result is a strain in which the target sequence is cleanly deleted, leaving no trace of the pUIC3 vector. See Text S3 for more details on each genotype, and the engineering process.

ACKNOWLEDGEMENTS

We thank Paul Rainey, Jesús Mercado-Blanco, and Steven Lindow for the kind gifts of *P. fluorescens* SBW25, *P. simiae* PICF7, and *P. fluorescens* A506, respectively. We thank Frederic Bertels for assistance with building the *Pseudomonas* phylogenetic tree. Funds were received from the Max Planck Society, and the International Max Planck Research School for Evolutionary Biology (IMPRS-EB). Open access funding enabled and organized by ProjektDEAL.

AUTHOR CONTRIBUTIONS

Anuradha Mukherjee and Jenna Gallie conceived the research. All authors performed the experiments and data analyses. Anuradha Mukherjee and Jenna Gallie wrote the manuscript, and all authors commented.

DATA AVAILABILITY STATEMENT

The data that supports the findings of this study are available in the supplementary material of this article. Whole genome sequencing data is openly available in the NCBI Sequencing Read Archive at [https://www.ncbi.nlm.nih.gov/sra], under PRJNA730882.

ORCID

Anuradha Mukherjee https://orcid.org/0000-0002-4120-6596
Gunda Dechow-Seligmann https://orcid.org/0000-0002-2824-9057
Jenna Gallie https://orcid.org/0000-0003-2918-0925

REFERENCES

Abraham, J.M., Freitag, C.S., Clements, J.R. & Eisenstein, B.I. (1985) An invertible element of DNA controls phase variation of type 1 fimbriae of *Escherichia coli*. *Proceedings of the National Academy of Sciences of the United States of America*, *82*, 5724–5727. https://doi.org/10.1073/pnas.82.17.5724

Amikam, D. & Galperin, M.Y. (2006) PilZ domain is part of the bacterial c-di-GMP binding protein. *Bioinformatics*, *22*, 3–6. https://doi.org/10.1093/bioinformatics/bti739

Anderson, P. & Roth, J. (1981) Spontaneous tandem genetic duplications in *Salmonella typhimurium* arise by unequal recombination between rRNA (*rrn*) cistrons. *Proceedings of the National Academy of*

Sciences of the United States of America, *78*, 3113–3117. https://doi.org/10.1073/pnas.78.5.3113

Anderson, R.P. & Roth, J.R. (1977) Tandem genetic duplications in phage and bacteria. *Annual Review of Microbiology*, *31*, 473–505. https://doi.org/10.1146/annurev.mi.31.100177.002353

Ardré, M., Dufour, D. & Rainey, P.B. (2019) Causes and biophysical consequences of cellulose production by *Pseudomonas fluorescens* SBW25 at the air-liquid interface. *Journal of Bacteriology*, *201*, e00110-19. https://doi.org/10.1128/JB.00110-19

Ayan, G.B., Park, H.J. & Gallie, J. (2020) The birth of a bacterial tRNA gene by large-scale, tandem duplication events. *eLife*, *9*, e57947. https://doi.org/10.7554/eLife.57947

Bantinaki, E., Kassen, R., Knight, C.G., Robinson, Z., Spiers, A.J. & Rainey, P.B. (2007) Adaptive divergence in experimental populations of *Pseudomonas fluorescens*. III. Mutational origins of wrinkly spreader diversity. *Genetics*, *176*, 441–453. https://doi.org/10.1534/genetics.106.069906

Baraquet, C., Murakami, K., Parsek, M.R. & Harwood, C.S. (2012) The FleQ protein from *Pseudomonas aeruginosa* functions as both a repressor and an activator to control gene expression from the *pel* operon promoter in response to c-di-GMP. *Nucleic Acids Research*, *40*, 7207–7218. https://doi.org/10.1093/nar/gks384

Barends, T.R.M., Hartmann, E., Griese, J.J., Beitlich, T., Kirienko, N.V., Ryjenkov, D.A. et al. (2009) Structure and mechanism of a bacterial light-regulated cyclic nucleotide phosphodiesterase. *Nature*, *459*, 1015–1018. https://doi.org/10.1038/nature07966

Barrick, J.E., Colburn, G., Deatherage, D.E., Traverse, C.C., Strand, M.D., Borges, J.J. et al. (2014) Identifying structural variation in haploid microbial genomes from short-read resequencing data using *breseq*. *BMC Genomics*, *15*, 1039. https://doi.org/10.1186/1471-2164-15-1039

Beaumont, H.J.E., Gallie, J., Kost, C., Ferguson, G.C. & Rainey, P.B. (2009) Experimental evolution of bet hedging. *Nature*, *462*, 90–93. https://doi.org/10.1038/nature08504

Bertels, F., Silander, O.K., Pachkov, M., Rainey, P.B. & Nimwegen, E.V. (2014) Automated reconstruction of whole-genome phylogenies from short-sequence reads. *Molecular Biology and Evolution*, *31*, 1077–1088. https://doi.org/10.1093/molbev/msu088

Boehm, A., Steiner, S., Zaehringer, F., Casanova, A., Hamburger, F., Ritz, D. et al. (2009) Second messenger signalling governs *Escherichia coli* biofilm induction upon ribosomal stress. *Molecular Microbiology*, *72*, 1500–1516. https://doi.org/10.1111/j.1365-2958.2009.06739.x

Borlee, B.R., Goldman, A.D., Murakami, K., Samudrala, R., Wozniak, D.J. & Parsek, M.R. (2010) *Pseudomonas aeruginosa* uses a cyclic-di-GMP-regulated adhesin to reinforce the biofilm extracellular matrix. *Molecular Microbiology*, *75*, 827–842. https://doi.org/10.1111/j.1365-2958.2009.06991.x

Chan, C., Paul, R., Samoray, D., Amiot, N.C., Giese, B., Jenal, U. et al. (2004) Structural basis of activity and allosteric control of diguanylate cyclase. *Proceedings of the National Academy of Sciences of the United States of America*, *101*, 17084–17089. https://doi.org/10.1073/pnas.0406134101

Chen, A.G.Y., Sudarsan, N. & Breaker, R.R. (2011) Mechanism for gene control by a natural allosteric group I ribozyme. *RNA*, *17*, 1967–1972. https://doi.org/10.1261/rna.2757311

Colvin, K.M., Irie, Y., Tart, C.S., Urbano, R., Whitney, J.C., Ryder, C. et al. (2012) The Pel and Psl polysaccharides provide *Pseudomonas aeruginosa* structural redundancy within the biofilm matrix. *Environmental Microbiology*, *14*, 1913–1928. https://doi.org/10.1111/j.1462-2920.2011.02657.x

Costerton, J.W., Stewart, P.S. & Greenberg, E.P. (1999) Bacterial biofilms: a common cause of persistent infections. *Science*, *284*, 1318–1322. https://doi.org/10.1126/science.284.5418.1318

D'Argenio, D.A., Calfee, M.W., Rainey, P.B. & Pesci, E.C. (2002) Autolysis and autoaggregation in *Pseudomonas aeruginosa* colony morphology mutants. *Journal of Bacteriology*, *184*, 6481–6489. https://doi.org/10.1128/JB.184.23.6481-6489.2002

Davey, M.E. & O'Toole, G.A. (2000) Microbial biofilms: from ecology to molecular genetics. *Microbiology and Molecular Biology Reviews*, *64*, 847–867. https://doi.org/10.1128/MMBR.64.4.847-867.2000

De Bolle, X., Bayliss, C.D., Field, D., van de Ven, T., Saunders, N.J., Hood, D.W. et al. (2000) The length of a tetranucleotide repeat tract in *Haemophilus influenzae* determines the phase variation rate of a gene with homology to type III DNA methyltransferases. *Molecular Microbiology*, *35*, 211–222. https://doi.org/10.1046/j.1365-2958.2000.01701.x

Deatherage, D.E. & Barrick, J.E. (2014) Identification of mutations in laboratory-evolved microbes from next-generation sequencing data using *breseq*. *Methods in Molecular Biology*, *1151*, 165–188. https://doi.org/10.1007/978-1-4939-0554-6_12

Duerig, A., Abel, S., Folcher, M., Nicollier, M., Schwede, T., Amiot, N. et al. (2009) Second messenger-mediated spatiotemporal control of protein degradation regulates bacterial cell cycle progression. *Genes & Development*, *23*, 93–104. https://doi.org/10.1101/gad.502409

Dybvig, K. & Yu, H. (1994) Regulation of a restriction and modification system via DNA inversion in *Mycoplasma pulmonis*. *Molecular Microbiology*, *12*, 547–560.

Friedman, L. & Kolter, R. (2004) Genes involved in matrix formation in *Pseudomonas aeruginosa* PA14 biofilms. *Molecular Microbiology*, *51*, 675–690. https://doi.org/10.1046/j.1365-2958.2003.03877.x

Gal, M., Preston, G.M., Massey, R.C., Spiers, A.J. & Rainey, P.B. (2003) Genes encoding a cellulosic polymer contribute toward the ecological success of *Pseudomonas fluorescens* SBW25 on plant surfaces. *Molecular Ecology*, *12*, 3109–3121. https://doi.org/10.1046/j.1365-294x.2003.01953.x

Gallie, J., Bertels, F., Remigi, P., Ferguson, G.C., Nestmann, S. & Rainey, P.B. (2019) Repeated phenotypic evolution by different genetic routes in *Pseudomonas fluorescens* SBW25. *Molecular Biology and Evolution*, *36*, 1071–1085. https://doi.org/10.1093/molbev/msz040

Gallie, J., Libby, E., Bertels, F., Remigi, P., Jendresen, C.B., Ferguson, G.C. et al. (2015) Bistability in a metabolic network underpins the *de novo* evolution of colony switching in *Pseudomonas fluorescens*. *PLoS Biology*, *13*, e1002109. https://doi.org/10.1371/journal.pbio.1002109

Giddens, S.R., Jackson, R.W., Moon, C.D., Jacobs, M.A., Zhang, X.X., Gehrig, S.M. et al. (2007) Mutational activation of niche-specific genes provides insight into regulatory networks and bacterial function in a complex environment. *Proceedings of the National Academy of Sciences of the United States of America*, *104*, 18247–18252. https://doi.org/10.1073/pnas.0706739104

Goymer, P., Kahn, S.G., Malone, J.G., Gehrig, S.M., Spiers, A.J. & Rainey, P.B. (2006) Adaptive divergence in experimental populations of *Pseudomonas fluorescens*. II. Role of the GGDEF regulator WspR in evolution and development of the wrinkly spreader phenotype. *Genetics*, *173*, 515–526. https://doi.org/10.1534/genetics.106.055863

Guindon, S. & Gascuel, O. (2003) A simple, fast, and accurate algorithm to estimate large phylogenies by maximum likelihood. *Systematic Biology*, *52*, 696–704. https://doi.org/10.1080/10635150390235520

Hagen, M.J., Stockwell, V.O., Whistler, C.A., Johnson, K.B. & Loper, J.E. (2009) Stress tolerance and environmental fitness of *Pseudomonas fluorescens* A506, which has a mutation in *rpoS*. *Phytopathology*, *99*, 679–688. https://doi.org/10.1094/PHYTO-99-6-0679

Hickman, J.W. & Harwood, C.S. (2008) Identification of FleQ from *Pseudomonas aeruginosa* as a c-di-GMP-responsive transcription factor. *Molecular Microbiology*, *69*, 376–389. https://doi.org/10.1111/j.1365-2958.2008.06281.x

Hickman, J.W., Tifrea, D.F. & Harwood, C.S. (2005) A chemosensory system that regulates biofilm formation through modulation of cyclic diguanylate levels. *Proceedings of the National Academy of Sciences*

of the United States of America, *102*, 14422–14427. https://doi.org/10.1073/pnas.0507170102

Ho, S.N., Hunt, H.D., Horton, R.M., Pullen, J.K. & Pease, L.R. (1989) Site-directed mutagenesis by overlap extension using the polymerase chain reaction. *Gene*, *77*, 51–59. https://doi.org/10.1016/0378-1119(89)90358-2

Jacobs, M.A., Alwood, A., Thaipisuttikul, I., Spencer, D., Haugen, E., Ernst, S. et al. (2003) Comprehensive transposon mutant library of *Pseudomonas aeruginosa*. *Proceedings of the National Academy of Sciences of the United States of America*, *100*, 14339–14344. https://doi.org/10.1073/pnas.2036282100

Jennings, L.K., Storek, K.M., Ledvina, H.E., Coulon, C., Marmont, L.S., Sadovskaya, I. et al. (2015) Pel is a cationic exopolysaccharide that cross-links extracellular DNA in the *Pseudomonas aeruginosa* biofilm matrix. *Proceedings of the National Academy of Sciences of the United States of America*, *112*, 11353–11358. https://doi.org/10.1073/pnas.1503058112

King, E.O., Ward, M.K. & Raney, D.E. (1954) Two simple media for the demonstration of pyocyanin and fluorescin. *The Journal of Laboratory and Clinical Medicine*, *44*, 301–307. PubMed ID: 13184240.

Koza, A., Hallett, P.D., Moon, C.D. & Spiers, A.J. (2009) Characterization of a novel air–liquid interface biofilm of *Pseudomonas fluorescens* SBW25. *Microbiology*, *155*, 1397–1406. https://doi.org/10.1099/mic.0.025064-0

Koza, A., Jerdan, R., Cameron, S. & Spiers, A.J. (2020) Three biofilm types produced by a model pseudomonad are differentiated by structural characteristics and fitness advantage. *Microbiology*, *166*, 707–716. https://doi.org/10.1099/mic.0.000938

Koza, A., Kuśmierska, A., McLaughlin, K., Moshynets, O. & Spiers, A.J. (2017) Adaptive radiation of *Pseudomonas fluorescens* SBW25 in experimental microcosms provides an understanding of the evolutionary ecology and molecular biology of A-L interface biofilm formation. *FEMS Microbiology Letters*, *364*, fnx109. https://doi.org/10.1093/femsle/fnx109

Koza, A., Moshynets, O., Otten, W. & Spiers, A.J. (2011) Environmental modification and niche construction: developing O_2 gradients drive the evolution of the wrinkly spreader. *The ISME Journal*, *5*, 665–673. https://doi.org/10.1038/ismej.2010.156

Lee, V.T., Matewish, J.M., Kessler, J.L., Hyodo, M., Hayakawa, Y. & Lory, S. (2007) A cyclic-di-GMP receptor required for bacterial exopolysaccharide production. *Molecular Microbiology*, *65*, 1474–1484. https://doi.org/10.1111/j.1365-2958.2007.05879.x

Leinonen, R., Sugawara, H. & Shumway, M. (2011) The sequence read archive. *Nucleic Acids Research*, *39*, D19–D21. https://doi.org/10.1093/nar/gkq1019

Li, Z., Chen, J.-H., Hao, Y. & Nair, S.K. (2012) Structures of the PelD cyclic diguanylate effector involved in pellicle formation in *Pseudomonas aeruginosa* PAO1. *Journal of Biological Chemistry*, *287*, 30191–30204. https://doi.org/10.1074/jbc.M112.378273

Liang, Z.-X. (2015) The expanding roles of c-di-GMP in the biosynthesis of exopolysaccharides and secondary metabolites. *Natural Product Reports*, *32*, 663–683. https://doi.org/10.1039/c4np00086b

Lind, P.A., Farr, A.D. & Rainey, P.B. (2017) Evolutionary convergence in experimental *Pseudomonas* populations. *The ISME Journal*, *11*, 589–600. https://doi.org/10.1038/ismej.2016.157

Lind, P.A., Libby, E., Herzog, J. & Rainey, P.B. (2019) Predicting mutational routes to new adaptive phenotypes, *eLife*, *8*, e38822. https://doi.org/10.7554/eLife.38822

Loper, J.E., Hassan, K.A., Mavrodi, D.V., Davis, E.W., Lim, C.K., Shaffer, B.T. et al. (2012) Comparative genomics of plant-associated *Pseudomonas* spp.: insights into diversity and inheritance of traits involved in multitrophic interactions. *PLoS Genetics*, *8*, e1002784. https://doi.org/10.1371/journal.pgen.1002784

Malone, J.G., Jaeger, T., Spangler, C., Ritz, D., Spang, A., Arrieumerlou, C. et al. (2010) YfiBNR mediates cyclic di-GMP dependent small colony variant formation and persistence in *Pseudomonas aeruginosa*. *PLoS Path*, *6*, e1000804. https://doi.org/10.1371/journal.ppat.1000804

Malone, J.G., Williams, R., Christen, M., Jenal, U., Spiers, A.J. & Rainey, P.B. (2007) The structure–function relationship of WspR, a *Pseudomonas fluorescens* response regulator with a GGDEF output domain. *Microbiology*, *153*, 980–994. https://doi.org/10.1099/mic.0.2006/002824-0

Manoil, C. (2000) Tagging exported proteins using *Escherichia coli* alkaline phosphatase gene fusions. *Methods in Enzymology*, *326*, 35–47. https://doi.org/10.1016/s0076-6879(00)26045-x

Martínez-García, P.M., Ruano-Rosa, D., Schilirò, E., Prieto, P., Ramos, C., Rodríguez-Palenzuela, P. et al. (2015) Complete genome sequence of *Pseudomonas fluorescens* strain PICF7, an indigenous root endophyte from olive (*Olea europaea L.*) and effective biocontrol agent against *Verticillium dahliae*. *Standards in Genomic Sciences*, *10*, 10. https://doi.org/10.1186/1944-3277-10-10

Matsuyama, B.Y., Krasteva, P.V., Baraquet, C., Harwood, C.S., Sondermann, H. & Navarro, M.V.A.S. (2016) Mechanistic insights into c-di-GMP–dependent control of the biofilm regulator FleQ from *Pseudomonas aeruginosa*. *Proceedings of the National Academy of Sciences of the United States of America*, *113*, E209–E218. https://doi.org/10.1073/pnas.1523148113

McDonald, M.J., Gehrig, S.M., Meintjes, P.L., Zhang, X.X. & Rainey, P.B. (2009) Adaptive divergence in experimental populations of *Pseudomonas fluorescens*. IV. Genetic constraints guide evolutionary trajectories in a parallel adaptive radiation. *Genetics*, *183*, 1041–1053. https://doi.org/10.1534/genetics.109.107110

Mercado-Blanco, J., Rodríguez-Jurado, D., Hervás, A. & Jiménez-Díaz, R.M. (2004) Suppression of Verticillium wilt in olive planting stocks by root-associated fluorescent *Pseudomonas spp*. *Biological Control*, *30*, 474–486. https://doi.org/10.1016/j.biocontrol.2004.02.002

Molina-Henares, M.A., Ramos-González, M.I., Daddaoua, A., Fernández-Escamilla, A.M. & Espinosa-Urgel, M. (2017) FleQ of *Pseudomonas putida* KT2440 is a multimeric cyclic diguanylate binding protein that differentially regulates expression of biofilm matrix components. *Research in Microbiology*, *168*, 36–45. https://doi.org/10.1016/j.resmic.2016.07.005

Montes-Osuna, N., Gómez-Lama Cabanás, C., Valverde-Corredor, A., Berendsen, R.L., Prieto, P. & Mercado-Blanco, J. (2021) Assessing the involvement of selected phenotypes of *Pseudomonas simiae* PICF7 in olive root colonization and biological control of *Verticillium dahliae*. *Plants*, *10*, 412. https://doi.org/10.3390/plants10020412

Moxon, R., Bayliss, C. & Hood, D. (2006) Bacterial contingency loci: the role of simple sequence DNA repeats in bacterial adaptation. *Annual Review of Genetics*, *40*, 307–333. https://doi.org/10.1146/annurev.genet.40.110405.090442

Nixon, B.T., Ronson, C.W. & Ausubel, F.M. (1986) Two-component regulatory systems responsive to environmental stimuli share strongly conserved domains with the nitrogen assimilation regulatory genes *ntrB* and *ntrC*. *Proceedings of the National Academy of Sciences of the United States of America*, *83*, 7850–7854. https://doi.org/10.1073/pnas.83.20.7850

Orsi, R.H., Bowen, B.M. & Wiedmann, M. (2010) Homopolymeric tracts represent a general regulatory mechanism in prokaryotes. *BMC Genomics*, *11*, 102. https://doi.org/10.1186/1471-2164-11-102

Paul, R., Weiser, S., Amiot, N.C., Chan, C., Schirmer, T., Giese, B. et al. (2004) Cell cycle-dependent dynamic localization of a bacterial response regulator with a novel di-guanylate cyclase output domain. *Genes & Development*, *18*, 715–727. https://doi.org/10.1101/gad.289504

Rainey, P.B. (1999) Adaptation of *Pseudomonas fluorescens* to the plant rhizosphere. *Environmental Microbiology*, *1*, 243–257. https://doi.org/10.1046/j.1462-2920.1999.00040.x

Rainey, P.B. & Rainey, K. (2003) Evolution of cooperation and conflict in experimental bacterial populations. *Nature*, *425*, 72–74. https://doi.org/10.1038/nature01906

Rainey, P.B. & Travisano, M. (1998) Adaptive radiation in a heterogeneous environment. *Nature*, *394*, 69–72. https://doi.org/10.1038/27900

Ramos-González, M.I., Travieso, M.L., Soriano, M.I., Matilla, M.A., Huertas-Rosales, Ó., Barrientos-Moreno, L. et al. (2016) Genetic dissection of the regulatory network associated with high c-di-GMP levels in *Pseudomonas putida* KT2440. *Frontiers in Microbiology*, *7*, 1093. https://doi.org/10.3389/fmicb.2016.01093

Rehm, B.H.A. (2010) Bacterial polymers: biosynthesis, modifications and applications. *Nature Reviews Microbiology*, *8*, 578–592. https://doi.org/10.1038/nrmicro2354

Reinders, A., Hee, C.-S., Ozaki, S., Mazur, A., Boehm, A., Schirmer, T. et al. (2016) Expression and genetic activation of cyclic di-GMP-specific phosphodiesterases in *Escherichia coli*. *Journal of Bacteriology*, *198*, 448–462. https://doi.org/10.1128/JB.00604-15

Remigi, P., Ferguson, G.C., McConnell, E., De Monte, S., Rogers, D.W. & Rainey, P.B. (2019) Ribosome provisioning activates a bistable switch coupled to fast exit from stationary phase. *Molecular Biology and Evolution*, *36*, 1056–1070. https://doi.org/10.1093/molbev/msz041

Richter, A.M., Possling, A., Malysheva, N., Yousef, K.P., Herbst, S., von Kleist, M. et al. (2020) Local c-di-GMP signaling in the control of synthesis of the *E. coli* biofilm exopolysaccharide pEtN-cellulose. *Journal of Molecular Biology*, *432*, 4576–4595. https://doi.org/10.1016/j.jmb.2020.06.006

Römling, U., Galperin, M.Y. & Gomelsky, M. (2013) Cyclic di-GMP: the first 25 years of a universal bacterial second messenger. *Microbiology and Molecular Biology Reviews*, *77*, 1–52. https://doi.org/10.1128/MMBR.00043-12

Ross, P., Weinhouse, H., Aloni, Y., Michaeli, D., Weinberger-Ohana, P., Mayer, R. et al. (1987) Regulation of cellulose synthesis in *Acetobacter xylinum* by cyclic diguanylic acid. *Nature*, *325*, 279–281. https://doi.org/10.1038/325279a0

Ryjenkov, D.A., Simm, R., Römling, U. & Gomelsky, M. (2006) The PilZ domain is a receptor for the second messenger c-di-GMP. *Journal of Biological Chemistry*, *281*, 30310–30314. https://doi.org/10.1074/jbc.C600179200

Schmidt, A.J., Ryjenkov, D.A. & Gomelsky, M. (2005) The ubiquitous protein domain EAL is a cyclic diguanylate-specific phosphodiesterase: enzymatically active and inactive EAL domains. *Journal of Bacteriology*, *187*, 4774–4781. https://doi.org/10.1128/JB.187.14.4774-4781.2005

Silby, M.W., Cerdeño-Tárraga, A.M., Vernikos, G.S., Giddens, S.R., Jackson, R.W., Preston, G.M. et al. (2009) Genomic and genetic analyses of diversity and plant interactions of *Pseudomonas fluorescens*. *Genome Biology*, *10*, R51. https://doi.org/10.1186/gb-2009-10-5-r51

Spiers, A.J. (2014) A mechanistic explanation linking adaptive mutation, niche change, and fitness advantage for the wrinkly spreader. *International Journal of Evolutionary Biology*, *2014*, 1–10. https://doi.org/10.1155/2014/675432

Spiers, A.J., Bohannon, J., Gehrig, S.M. & Rainey, P.B. (2003) Biofilm formation at the air-liquid interface by the *Pseudomonas fluorescens* SBW25 wrinkly spreader requires an acetylated form of cellulose. *Molecular Microbiology*, *50*, 15–27. https://doi.org/10.1046/j.1365-2958.2003.03670.x

Spiers, A.J., Kahn, S.G., Bohannon, J., Travisano, M. & Rainey, P.B. (2002) Adaptive divergence in experimental populations of *Pseudomonas fluorescens*. I. Genetic and phenotypic bases of wrinkly spreader fitness. *Genetics*, *161*, 33–46. https://doi.org/10.1093/genetics/161.1.33

Starkey, M., Hickman, J.H., Ma, L., Zhang, N., De Long, S., Hinz, A. et al. (2009) *Pseudomonas aeruginosa* rugose small-colony variants have adaptations that likely promote persistence in the cystic fibrosis lung. *Journal of Bacteriology*, *191*, 3492–3503. https://doi.org/10.1128/JB.00119-09

Steiner, S., Lori, C., Boehm, A. & Jenal, U. (2012) Allosteric activation of exopolysaccharide synthesis through cyclic di-GMP-stimulated protein–protein interaction. *The EMBO Journal*, *32*, 354–368. https://doi.org/10.1038/emboj.2012.315

Stock, A.M., Robinson, V.L. & Goudreau, P.N. (2000) Two-component signal transduction. *Annual Review of Biochemistry*, *69*, 183–215. https://doi.org/10.1146/annurev.biochem.69.1.183

Stockwell, V.O., Davis, E.W., Carey, A., Shaffer, B.T., Mavrodi, D.V., Hassan, K.A. et al. (2013) pA506, a conjugative plasmid of the plant epiphyte *Pseudomonas fluorescens* A506. *Applied Environmental Microbiology*, *79*, 5272–5282. https://doi.org/10.1128/AEM.01354-13

Stockwell, V.O., Johnson, K.B., Sugar, D. & Loper, J.E. (2010) Control of fire blight by *Pseudomonas fluorescens* A506 and *Pantoea vagans* C9–1 applied as single strains and mixed inocula. *Phytopathology*, *100*, 1330–1339. https://doi.org/10.1094/PHYTO-03-10-0097

Sudarsan, N., Lee, E.R., Weinberg, Z., Moy, R.H., Kim, J.N., Link, K.H. et al. (2008) Riboswitches in eubacteria sense the second messenger cyclic di-GMP. *Science*, *321*, 411–413. https://doi.org/10.1126/science.1159519

Tal, R., Wong, H.C., Calhoon, R., Gelfand, D., Fear, A.L., Volman, G. et al. (1998) Three *cdg* operons control cellular turnover of cyclic di-GMP in *Acetobacter xylinum*: genetic organization and occurrence of conserved domains in isoenzymes. *Journal of Bacteriology*, *180*, 4416–4425. https://doi.org/10.1128/JB.180.17.4416-4425.1998

Tiwari, A., Ray, J.C.J., Narula, J. & Igoshin, O.A. (2011) Bistable responses in bacterial genetic networks: designs and dynamical consequences. *Mathematical Biosciences*, *231*, 76–89. https://doi.org/10.1016/j.mbs.2011.03.004

Valentini, M. & Filloux, A. (2019) Multiple roles of c-di-GMP signaling in bacterial pathogenesis. *Annual Review of Microbiology*, *73*, 387–406. https://doi.org/10.1146/annurev-micro-020518-115555

Whitfield, G.B., Marmont, L.S., Bundalovic-Torma, C., Razvi, E., Roach, E.J., Khursigara, C.M. et al. (2020) Discovery and characterization of a Gram-positive Pel polysaccharide biosynthetic gene cluster. *PLoS Path*, *16*, e1008281. https://doi.org/10.1371/journal.ppat.1008281

Yaron, S. & Römling, U. (2014) Biofilm formation by enteric pathogens and its role in plant colonization and persistence. *Microbial Biotechnology*, *7*, 496–516. https://doi.org/10.1111/1751-7915.12186

Zhang, X.X. & Rainey, P.B. (2007) Genetic analysis of the histidine utilization (*hut*) genes in *Pseudomonas fluorescens* SBW25. *Genetics*, *176*, 2165–2176. https://doi.org/10.1534/genetics.107.075713

Zordan, R.E., Galgoczy, D.J. & Johnson, A.D. (2006) Epigenetic properties of white-opaque switching in *Candida albicans* are based on a self-sustaining transcriptional feedback loop. *Proceedings of the National Academy of Sciences of the United States of America*, *103*, 12807–12812. https://doi.org/10.1073/pnas.0605138103

SUPPORTING INFORMATION

Additional supporting information may be found in the online version of the article at the publisher's website.

How to cite this article: Mukherjee, A., Dechow-Seligmann, G. & Gallie, J. (2022) Evolutionary flexibility in routes to mat formation by *Pseudomonas*. *Molecular Microbiology*, 117, 394–410. https://doi.org/10.1111/mmi.14855